frontiers | Frontiers in Marine Science

TYPE Original Research
PUBLISHED 30 October 2024
DOI 10.3389/fmars.2024.1460657

OPEN ACCESS

EDITED BY
Selvaraj Kandasamy,
Central University of Tamil Nadu, India

REVIEWED BY
Xiting Liu,
Ocean University of China, China
Yuan-Pin Chang,
National Sun Yat-sen University, Taiwan

*CORRESPONDENCE
Yajuan Yuan
yuanyajuan@m.scnu.edu.cn
Wei Zhang
zwgmgs@foxmail.com

RECEIVED 08 July 2024
ACCEPTED 02 October 2024
PUBLISHED 30 October 2024

CITATION
Luo X, Yuan Y, Zhang W, Huang W, Ou S, Ji C and Cao J (2024) Methane seepage activities in the Qiongdongnan Basin since MIS2. *Front. Mar. Sci.* 11:1460657. doi: 10.3389/fmars.2024.1460657

Methane seepage activities in the Qiongdongnan Basin since MIS2

Xiaokang Luo[1,2], Yajuan Yuan[1,2]*, Wei Zhang[2,3]*, Wei Huang[2,3], Shimin Ou[1], Chunsheng Ji[2,3] and Jun Cao[2,3]

[1]School of Geography, South China Normal University, Guangzhou, China, [2]National Engineering Research Center of Gas Hydrate Exploration and Development, Guangzhou, China, [3]Sanya Institute of South China Sea Geology, Guangzhou Marine Geological Survey, China Geological Survey, Sanya, China

Gas hydrates are globally acknowledged as a significant strategic alternative energy source, and there is a consensus on the necessity to enhance their exploration. However, gas hydrates are highly prone to decomposition under variations in external environmental conditions, which can result in subsea methane seepage activities. Consequently, investigating subsea methane seepage activities holds substantial theoretical and practical significance for exploring gas hydrates. This paper evaluates the history of methane seepage activities in the Qiongdongnan Basin (QDNB) by analyzing the carbon and oxygen isotopic characteristics of benthic foraminifera and the geochemical properties of pore water from gravity sediment cores at sites QH-CL4 and QH-CL40. The results indicate that since the Marine isotope stage2 (MIS2), continuous micro-methane seepage activity has been present in the QDNB, characterized by a slight negative deviation in the carbon isotopes of benthic foraminifera. Methane seepage activity intensified during 14.6 ka BP and between 19.64–23.22 ka BP. This increase is thought to be associated with rising seawater temperature during the Bølling–Allerød interstadial and declining sea level during the Last Glacial Maximum, respectively. Moreover, current geochemical characteristics of pore water reveal strong methane seepage activity, with flux as high as 28.968 $mmol \cdot m^{-2} \cdot a^{-1}$. This ongoing activity has led to gas hydrate formation within shallow layers while also causing negative deviations in pore water salinity.

KEYWORDS

methane seepage activities, pore water, foraminifera, geochemistry, Qiongdongnan Basin

1 Introduction

Gas hydrates are ice-like crystalline substances formed by the combination of methane and other hydrocarbon gases with water under conditions of low temperature and high-pressure. They predominantly occur in terrestrial permafrost zones and continental marine sediments (Kvenvolden, 1995; Suess, 2014). Gas hydrate systems exist in a state of dynamic

equilibrium and are highly sensitive to environmental changes (Lemaitre et al., 2014). Variations in seabed temperature and pressure changes can induce the dissociation of gas hydrates, resulting in the release of hydrocarbon gases (Niemann et al., 2006; Boetius and Wenzhoefer, 2013; Kirschke et al., 2013). The methane released during this process may migrate or be ejected through surface sediments, triggering seafloor geological events that contribute to global climate change (Dickens et al., 1997; Dickens, 2001; Archer et al., 2009; Them et al., 2018), thereby significantly impacting the global carbon cycle and climate dynamics. Therefore, it is of great significance to study methane seepage activities in regions abundant in gas hydrates.

Foraminifera are sensitive to environmental changes and have emerged as an significant indicator of methane seepage activities throughout geological history (Tetard et al., 2017). The stable isotopes of their shells can effectively record the properties of the surrounding water, and the extremely light carbon isotope values in methane will affect the dissolved inorganic carbon in the water, thereby inducing a negative bias in the $\delta^{13}C$ of foraminifera shells (Burkett et al., 2018). Since the Quaternary, numerous gas hydrate events have been identified by negative $\delta^{13}C$ excursions in foraminiferal shells, with discoveries reported from various regions, including the Bay of Bengal (Cen et al., 2022; Clemens et al., 2023), the Svalbard margin in the North Atlantic (Dessandier et al., 2020; Melaniuk et al., 2022a), the California margin in the North Pacific (Rathburn et al., 2000; Hill et al., 2003), Hydrate Ridge in Oregon, North Pacific (Hill et al., 2004, the Pearl River Mouth Basin (Wan et al., 2018), and the Dongsha area (Huang et al., 2022).

The current active methane seepage can be identified through the geochemical characteristics of pore water. Methane released from the dissociation of deep gas hydrates interacts with sulfate ions (SO_4^{2-}) in pore water, undergoing the anaerobic oxidation of methane (AOM, Equation 1) (Borowski et al., 1999). During drilling, the dissociation of shallow hydrates directly injects fresh water into pore water, causing anomalies in pore water salinity (Hesse and Harrison, 1981). Therefore, sediment pore water is crucial for documenting ongoing methane seepage activities and indicating the presence of gas hydrates. Abnormal geochemical signatures in pore water have confirmed current methane seepage activities as well as their existence. Examples include the Taixinan Basin in the South China Sea (Ye et al., 2016; Bohrmann et al., 2023), the Okinawa Trough in the East Sea (Xu et al., 2021), the Ulleung Basin in the East Sea (Kim et al., 2013), the Svalbard margin in the North Atlantic (Hong et al., 2018), and the Cascadia margin (Haeckel et al., 2004; Malinverno et al., 2008).

$$CH_4 + SO_4^{2-} \rightarrow HCO_3^- + HS^- + H_2O \quad (1)$$

The Qiongdongnan Basin in the South China Sea is abundant in gas hydrate resources, which significantly influence methane seepage fluxes (Wei et al., 2019; Ye et al., 2019; Lai et al., 2021; Ren et al., 2022). The geochemical characteristics of pore water indicate ongoing methane seepage activities in this region (Feng et al., 2018a; Hu et al., 2019; Sun et al., 2019; Wan et al., 2020). Additionally, evidence from authigenic carbonates and pyrite suggests that historical dissociation events of gas hydrates have occurred (Miao et al., 2021; Zhang et al., 2023a). This study concentrates on the QH-CL4 and QH-CL40 sites in the Qiongdongnan Basin. By analyzing the carbon and oxygen isotopic characteristics of benthic foraminifera from gravity core samples, we aim to reconstruct the history of methane seepage since MIS2. Furthermore, we investigate current methane seepage activities through geochemical analysis of pore water, exploring their implications for natural gas hydrates in the region.

2 Geological setting

The study area is located in the Qiongdongnan Basin on the northern continental slope of the South China Sea (Figure 1). Structurally, it is situated in the southwestern part of the Songnan Low Uplift, extending from longitudes 108°40′ to 112°35′ E and latitudes 16°50′to 19°00′ N, covering an area of approximately 80,000 km² (Wang et al., 2015). The water depth in the Qiongdongnan Basin varies between 1600 m and 1800 m, with a geothermal gradient ranging from 65 to 113°C/km (Wei et al., 2019; Deng et al., 2021).

Previous studies indicate that the Qiongdongnan Basin underwent a rifting stage from the Eocene to the Oligocene, followed by a post-rift thermal subsidence stage from the Tertiary to the Quaternary, which has shaped the current sedimentary characteristics of the basin (Hu et al., 2013; Zhao et al., 2015). The sedimentary succession is composed of Eocene lacustrine mudstones, Oligocene lacustrine and shallow water sediments, and Miocene deep water deposits (Zhao et al., 2015). The Eocene lacustrine mudstone, formed during the early rift stage, is characterized by multiple depressions and uplifts controlled by faulting (Li et al., 2017a). The Oligocene Yacheng Formation, deposited during the late rifting stage, is recognized as a primary source rock for hydrocarbons in the basin. Miocene deep-water deposits, including the Sanya, Meishan, and Huangliu formations, consist predominantly of mudstone and sandstone, representing products of the subsidence stage, and are located in channel sandstone reservoirs within the basin (Zhang et al., 2020). These thick hydrocarbon source rocks are crucial for the natural gas formation. Rapid sedimentation during the Cenozoic led to deep burial and compaction of sediments, resulting in widespread overpressure in the basin (Shi et al., 2013). This overpressure has triggered the formation of mud diapirs and gas chimneys, which are extensively distributed in the deep water, providing crucial vertical migration pathways for hydrocarbons (Zhang et al., 2019a).

In 2018, Guangzhou Marine Geological Survey (GMGS) conducted the 5th China gas hydrate drilling expedition (GMGS5) in the northwestern South China Sea and massive gas hydrate were sampled during this cruise. The true amplitude was preserved in the processing to clearly interpret the seismic features associated with the gas hydrates, especially the Bottom Simulating Reflectors (BSRs) (Yoo et al., 2013). The gas hydrate drilling site, GMGS5-W7-2018, is situated atop a large gas chimney, which originated from a low uplift (Figure 2). BSRs appeared on the top of or flank of the gas chimney area.

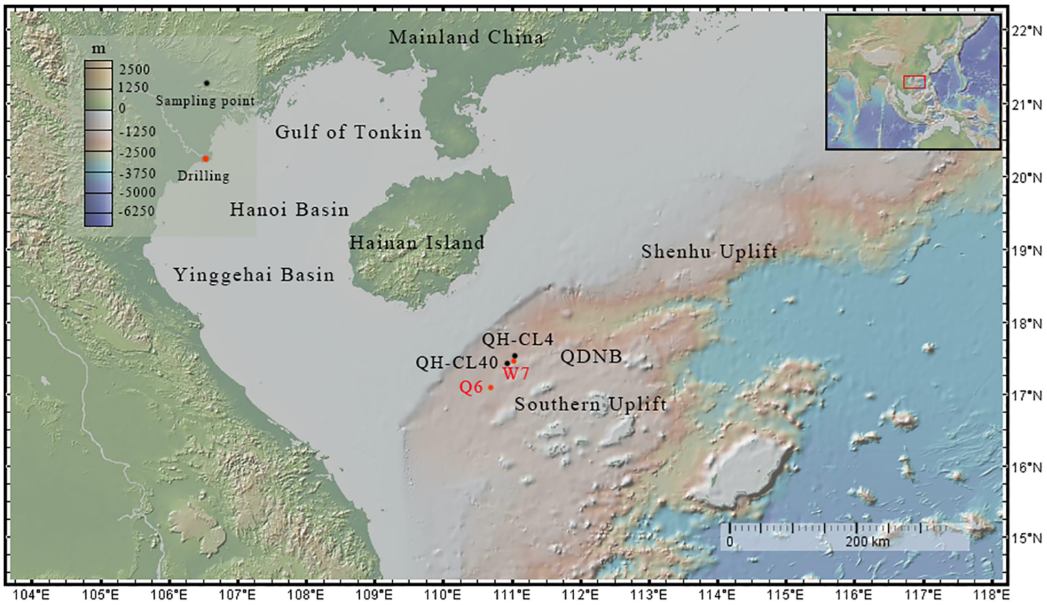

FIGURE 1
Location of the Qiongdongnan Basin and drilling location (The base map was modified after Ryan et al., 2009, with the drilling location of Q6 from Miao et al., 2021).

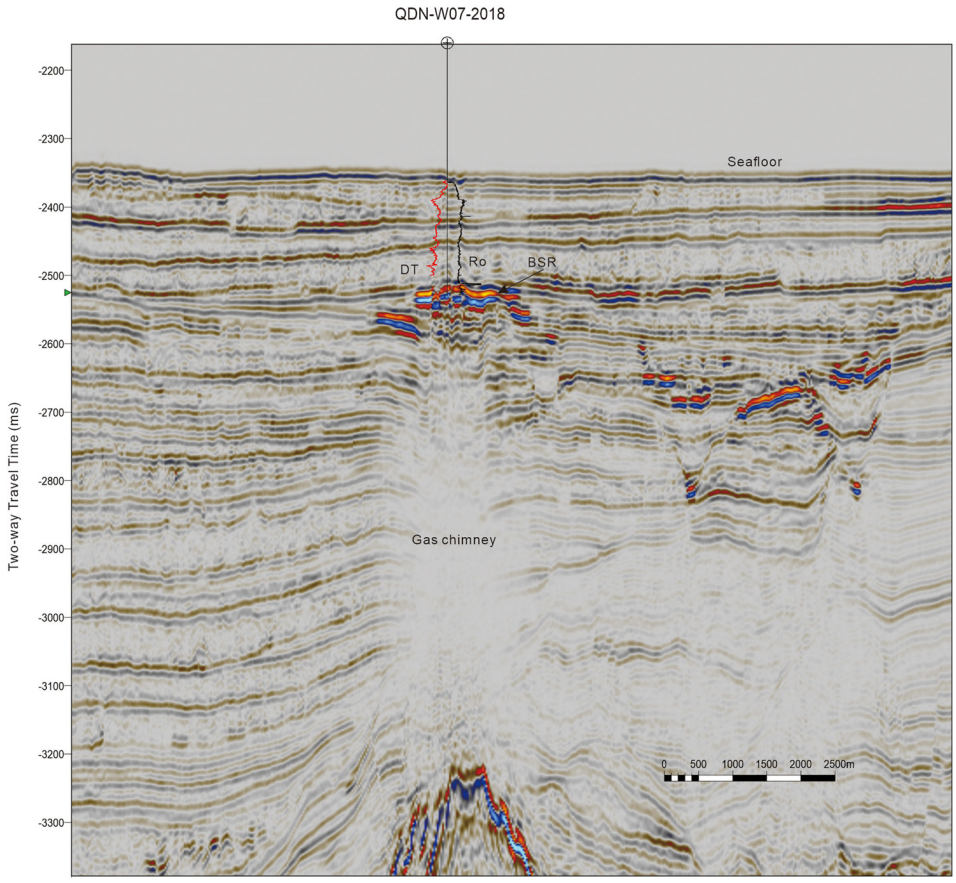

FIGURE 2
Seismic profiles across W07 with interpretations.

3 Materials and methods

3.1 Samples

The samples for this study were collected from the QH-CL4 and QH-CL40 sites during the fifth hydrate drilling expedition (GMGS5) by the Guangzhou Marine Geological Survey. Located near drilling site GMGS5-W7-2018 (Figure 1), these samples were obtained using large gravity piston cores. Each core measures 4.8 meters in length and was retrieved from a depth of approximately 1766 m. The cores primarily consist of light gray silty clay, with sections exhibiting greenish-gray silty clay (Liang et al., 2024).

Upon arrival on deck, pore water was extracted from the sediment cores of QH-CL4 and QH-CL40. The bottom 5-10 cm of each gravity piston core sample was removed, while the remaining samples were processed at intervals of 60 cm using a vacuum extraction device, yielding a total of 16 pore water samples. These samples were subsequently sealed in PTFE bottles and stored at 4°C for preservation.

3.2 Analytical methods

Following sample collection, the cores were transported to an indoor laboratory for further analysis. The frozen sediment samples were placed in a vacuum freeze-dryer for 72 hours, with the cold trap set to a minimum temperature of -80°C and the vacuum maintained at 0 Pa. After the samples were fully dried, they were sealed and stored under freezing conditions for future experiments.

Key tests include scanning electron microscopic (SEM) observation of foraminifera, stable isotope analysis of foraminifera, determination of major anions and cations in pore waters and Total organic carbon (TOC) in sediments.

The sediment samples were dried using a freeze dryer and preprocessed following standard micropaleontological methods. Fresh, uncontaminated benthic foraminifera species *Cibicidoides wuellerstorfi* (*C. weullerstorfi*) were selected from samples larger than 250μm for subsequent testing.

The foraminifera samples were coated with a gold film and examined using a field emission scanning electron microscope (FE-SEM TESCAN Mira3) at a voltage of 5kV. Comprehensive observations and secondary electron imaging were conducted for detailed analysis.

Fresh, uncontaminated fossils of *Cibicidoides wuellerstorfi* were cleaned with ≥99.7% anhydrous alcohol using a Branson 200 ultrasonic cleaner at 40KHz for 10-15 seconds. After removing the cloudy liquid, the samples were dried at 60°C for 5 hours. They were then placed in sample vials of a Kiel IV carbonate preparation device, dissolved in phosphoric acid at 70°C to release CO_2, and analyzed for oxygen and carbon isotope ratios using a MAT253 mass spectrometer. This analysis was conducted at the State Key Laboratory of Marine Geology at Tongji University, with precision verified using the NBS19 standard. Results were correlated to the international PDB scale.

TOC in the sediment samples was tested using a Heraeus CHN-O Rapid elemental analyzer (Germany). Prior to testing, an appropriate amount of sediment was selected, and excess 10% HCl was added to remove calcium carbonate. The samples were then repeatedly washed with distilled water until neutral, followed by drying in an oven at 50°C. The precision and accuracy of the TOC analyzer are better than 3%. The experiments were conducted at the Guangzhou Institute of Geochemistry, Chinese Academy of Sciences.

The pore water samples were transported to the State Key Laboratory of Organic Geochemistry at the Guangzhou Institute of Geochemistry for anion and cation concentration analysis. Anions concentrations were measured using a Thermo Fisher DIONEX AQUION RFIC ion chromatograph, while cations concentrations were analyzed with a Thermo Fisher ICS900 ion chromatograph. The analyses followed the standards HJ84-2016 for inorganic anions and HJ 812-2016 for soluble cations in water quality. The detection limits were 0.007 mg/L for Cl^-, 0.018 mg/L for Br^- and SO_4^{2-}, and 0.03 mg/L for Na^+, K^+, Mg^{2+}, and Ca^{2+}, with a precision requirement of ≤5%.

3.3 Methane seepage flux calculation method

The calculation of methane seepage flux follows Fick's first law:

$$J = -\phi D_s \frac{\partial C}{\partial x} \quad (2)$$

Where J denotes the ion diffusion flux (mmol×m^{-2}×a^{-1}); ϕ is the sediment porosity; D_s is the diffusion coefficient in sediment (m^{-2}×s^{-1}), which can be calculated as $D_s = \frac{D_0}{1-\ln \phi^2}$; D_0 is the free diffusion coefficient in seawater (m^{-2}×s^{-1}), C is the ion concentration in pore water (mmol/L), x is the sediment depth (m). For this study, the bottom water temperature at the research site is approximately 5°C (Wei et al., 2019), and the porosity is 75% (Feng et al., 2018a). The diffusion coefficient of SO_4^{2-} at 5°C 5.72×$10^{-10}$$m^{-2}$×$s^{-1}$ (Schulz et al., 2006).

4 Result

4.1 Stable carbon and oxygen isotope characteristics of foraminifera

The carbon and oxygen isotope test results for *Cibicidoides wuellerstorfi* (Figure 3) indicate the $\delta^{18}O$ values of this species range from 2.254‰ to 3.928‰ for QH-CL4 and from 2.302‰ to 4.249‰ for QH-CL40, with average values of 3.110‰ and 3.347‰, respectively. Both cores exhibit lighter $\delta^{18}O$ values in their upper sections, which correspond precisely to the MIS1 period. Similarly, the $\delta^{13}C$ values vary between -0.802‰ to 0.021‰ for QH-CL4 and -1.039‰ to -0.01‰ for QH-CL40, yielding mean values of -0.357‰ and -0.399‰, respectively.

Notably, carbon isotopes display varying degrees of negative shifts in two stages: Stage 1 (at a depth of 1.8 m) and Stage 2 (between depths of 3 to 4.2 m). In Stage 1, the $\delta^{13}C$ of foraminifera shells at site CL4 decreased to -0.802‰, approximately 0.5‰ lower

10.3389/fmars.2024.1460657

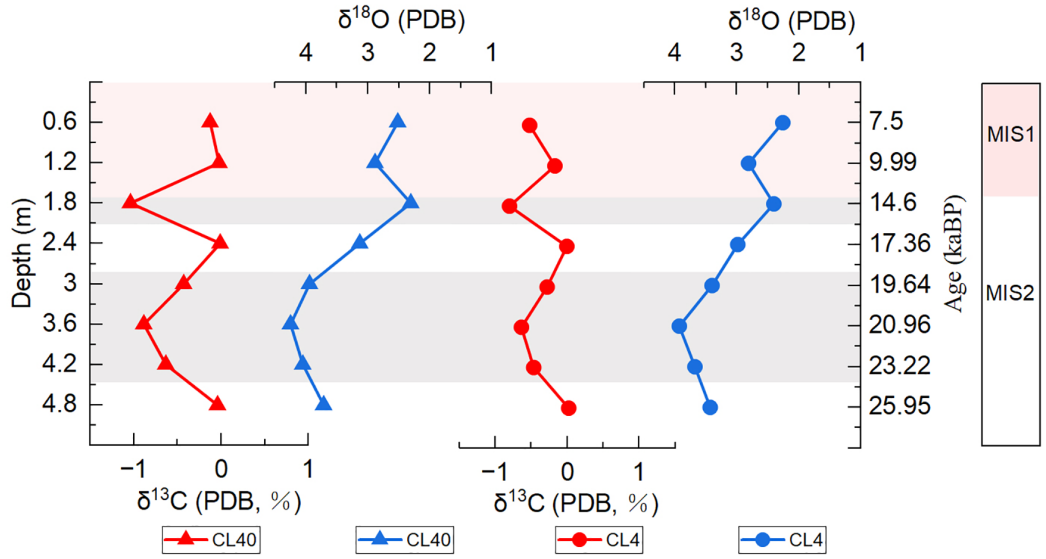

FIGURE 3
Stable isotope characteristics of the benthic foraminifera *C. wuellerstorfi* from sites QH-CL4 and QH-CL40. The shaded areas in the figure represent possible stages of enhanced methane seepage.

than the average, while at site CL40, it dropped to -1.039‰, representing a decrease of 0.7‰ from the average. In Stage 2, the $\delta^{13}C$ at CL4 ranged from -0.636‰ to -0.021‰, with an average of -0.36‰, while CL40 values ranged from -0.885‰ to -0.041‰, averaging -0.52‰. Overall, the carbon isotopes at both sites display a negative correlation with oxygen isotopes, although a positive correlation is observed at 1.8m.

The stratigraphic ages for these stations were initially determined using opto-luminescence dating data from nearby stations like W07 (Liang et al., 2024). However, due to the absence of data for the upper 0 to 1.8 meters, we referenced dating data from the Q6 station in the Qiongdongnan Basin (Miao et al., 2021). This provided eight age control points, which were utilized to estimate sedimentation rate changes for the two gravity piston core samples using a linear method (Table 1). These calculations facilitated the conversion of each sample's depth into its corresponding age (Table 2).

TABLE 1 Estimated sedimentation rates at various stages based on data from 8 age control points.

Stage	Depth range (m)	Age range (kaBP)	sedimentation rate (cm/ka)
1	0.11~0.61	2.17~7.61	9.19
2	0.61~1.07	7.61~9.91	20.00
3	1.07~1.33	9.91~10.07	162.50
4	1.33~1.8	10.07~14.6	10.38
5	1.8~2.8	14.6~19.2	21.74
6	2.8~3.8	19.2~21.4	45.45
7	3.8~4.9	21.4~26.4	22

4.2 Pore water ion concentration characteristics

The analysis of ion concentrations in pore water from QH-CL4 sediment shows significant variation with depth (Figure 4). Specifically, the Na^+ concentrations range from 101 to 467 mmol/L, averaging 336 mmol/L. The K^+ concentrations vary between 2.38 and 12.1 mmol/L, with a mean of 8.85 mmol/L. The divalent cations Mg^{2+} and Ca^{2+} also show characteristic distributions. Mg^{2+} concentrations range from 10.6 to 56.4 mmol/L, averaging 43.5 mmol/L. Meanwhile, Ca^{2+} concentrations fluctuate between 3.25 and 14.3 mmol/L, with a mean value of 10.4 mmol/L. Among the anions, Cl^- concentrations vary from 121 to 556 mmol/L, averaging 440 mmol/L. Additionally, Br^- concentrations range from 1.27 to 1.45 mmol/L, averaging 1.36 mmol/L, while SO_4^{2-} concentrations vary from 9.57 to 29.5 mmol/L, averaging 22.2 mmol/L.

The vertical variations in cation and anion concentrations at the study site exhibit similar patterns, with notable negative anomalies at depths of 1.8m, 3.6m, and 4.8m. For instance, chloride (Cl^-) concentrations in the upper sediment layers (0-1.2m) remain stable at around 556 mmol/L, close to seawater salinity (Staudigel et al., 1998). Starting at 1.2m, Cl^- concentration declines to 416 mmol/L at 1.8m, then rebounds to 528 mmol/L at 2.4m, and drops sharply to a low of 121 mmol/L at 3.6m. This suggests significantly lower Cl^- levels between 1.8m and 3.6m compared to standard seawater. From 3.6m to 4.2m, the concentration gradually returns to normal levels.

The ion concentrations in pore water from QH-CL40 sediment exhibit notable variations (Figure 5). Sodium (Na^+) ranges from 435 to 481 mmol/L, averaging 473 mmol/L, while potassium (K^+) varies between 10.9 and 12.1 mmol/L, averaging 11.7 mmol/L. Similarly, magnesium (Mg^{2+}) concentrations range from 49.5 to 56.4 mmol/L, averaging 52.8 mmol/L, and calcium (Ca^{2+}) fluctuates between 5.91 and 9.93 mmol/L, with an average of 8.57 mmol/L.

10.3389/fmars.2024.1460657

TABLE 2 Stratigraphic ages at various depths at sites QH-CL4 and QH-CL40 calculated based on sedimentation rates.

Depth (m)	Age (kaBP)
0.6	7.5
1.2	9.99
1.8	14.6
2.4	17.36
3	19.64
3.6	20.96
4.2	23.22
4.8	25.95

Chloride (Cl^-) concentrations range from 516.5 to 565.7 mmol/L, averaging 554.1 mmol/L, while bromide (Br^-) shows slight variations, ranging from 1.69 to 1.77 mmol/L, averaging 1.73 mmol/L. Sulfate (SO_4^{2-}) concentrations vary between 13.96 and 30.4 mmol/L, averaging 21.5 mmol/L.

At a depth of 0.6 meters, the sulfate (SO_4^{2-}) concentration measures approximately 30.4 mmol/L, consistent with typical seawater values (Staudigel et al., 1998). Deeper into the sediment, sulfate concentration gradually declines in a gradient, reaching 19.2 mmol/L at 4.8 meters. Notably, calcium (Ca^{2+}) follows a similar downward trend as sulfate. Meanwhile, other ion concentrations remain within typical seawater ranges.

4.3 Total organic carbon content

Total organic carbon values are presented in Table 3. At site CL4, the TOC content in the sediment ranged from 0.61% to 0.76%, with an average of 0.701%. The surface sediments on the seafloor exhibited the highest TOC content at 0.76%, while the TOC levels in the remaining layers were above 0.60%. At site CL40, TOC contents varied between 0.65% and 0.79%, averaging 0.7225%. Overall, the TOC contents at both sites were comparable and showed little variation with depth.

5 Discussion

5.1 Negative carbon isotope excursions of benthic foraminifera and methane seepage activities

Cibicidoides wuellerstorfi, an epifaunal benthic foraminifera species, is primarily influenced by bottom water, making it well-suited for reconstructing $\delta^{13}C$ values of dissolved inorganic carbon (DIC) in bottom waters (McCorkle et al., 1990; Wollenburg et al., 2015). This species typically attaches to structures above the seafloor (Melaniuk et al., 2022b) and shows minimal absolute changes in shell structure due to methane seepage. Although the negative deviation in its isotopic values is not pronounced, its broad oceanographic and stratigraphic range allows it to effectively

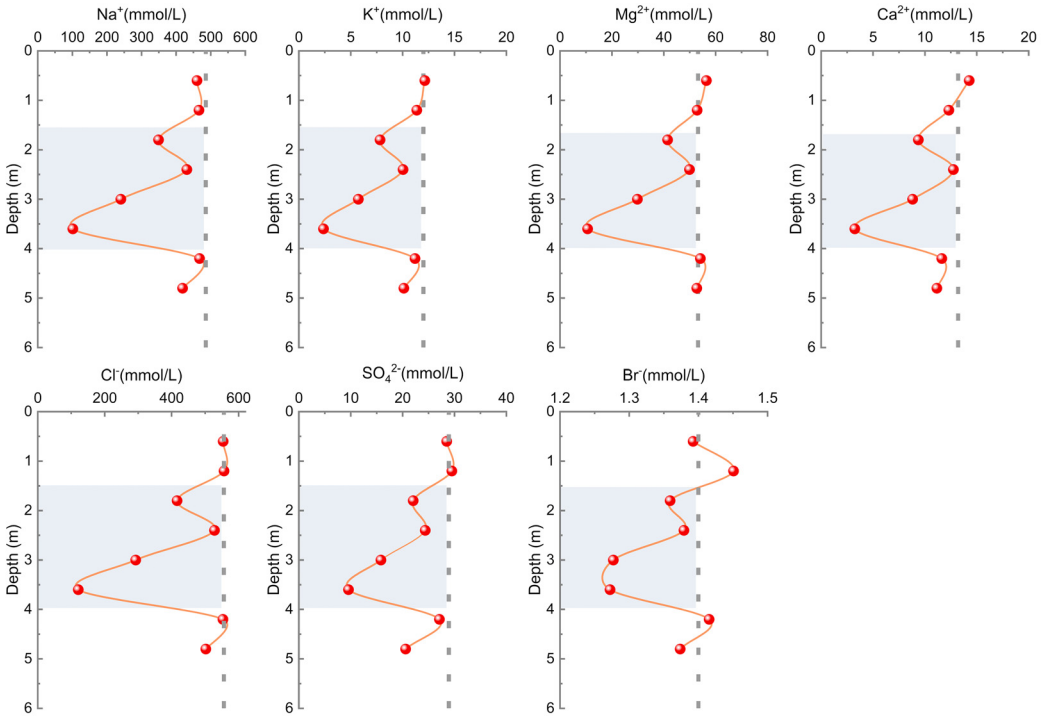

FIGURE 4
Profiles of pore water geochemical parameters of site QH-CL4. The shaded areas in the figure represent the layers with abnormal ion concentration, indicating the presence or suspected presence of gas hydrate. The dark gray dashed line represents the typical seawater concentration, with data from (Staudigel et al., 1998).

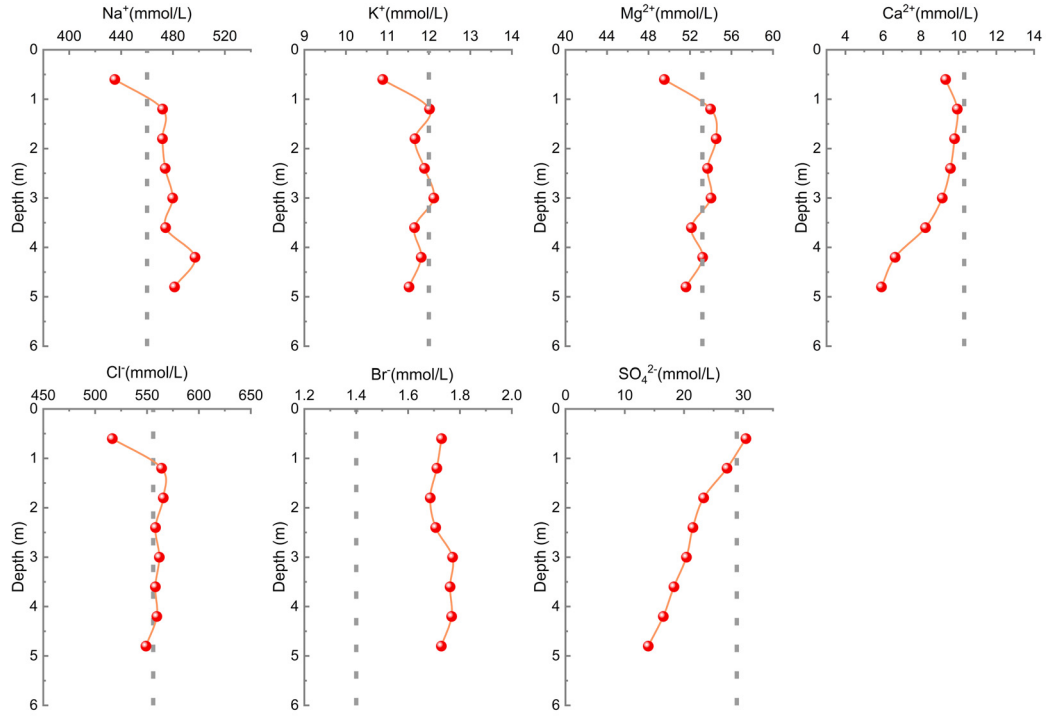

FIGURE 5
Profiles of pore water geochemical parameters of site QH-CL40. The dark gray dashed line represents the typical seawater concentration, with data from (Staudigel et al., 1998).

indicate methane leakage activity (Mackensen et al., 2006; Wollenburg et al., 2015; Mackensen et al., 2017; Burkett et al., 2018; Su et al., 2020; Melaniuk et al., 2022a; Weldeab et al., 2022). Studies have shown that in non-methane seep areas, the $\delta^{13}C$ values of *C. wuellerstorfi* range from -0.9‰ to 1.92‰, with an average of 0.217‰, and $\delta^{18}O$ values range from 1.38‰ to 4.09‰, with an average of 2.56‰. In contrast, in methane seep areas, the $\delta^{13}C$ values range from -1.39‰ to 1.31‰, with an average of -0.0685‰, and $\delta^{18}O$ values range from 1.38‰ to 4.09‰, with an average of 2.62‰ (Kubota et al., 2015; Mackensen et al., 2017; Scheiner et al., 2018; Cen et al., 2022; Dou et al., 2022). Overall, *C. wuellerstorfi* shows a slight negative shift in $\delta^{13}C$ and a positive shift in $\delta^{18}O$ in methane seep environments. The formation of hydrates preferentially incorporates $\delta^{18}O$-rich water, and their decomposition releases heavier $\delta^{18}O$, altering the surrounding pore water's oxygen isotopic composition and influencing the oxygen isotope composition of foraminifera (Kvenvolden, 1993; Mackensen et al., 2006). In a non-seep marine environment in the South China Sea, the $\delta^{13}C$ values of epifaunal benthic foraminifera *Cibicidoides wuellerstorfi* range from -0.73‰ to 1.53‰, with an average of 0.113‰ (Cheng et al., 2005). In this study, the average $\delta^{13}C$ values at sites QH-CL4 and QH-CL40 were -0.199‰ and 0.0224‰, respectively, with $\delta^{18}O$ values averaging 2.63‰ and 2.66‰. These shifts suggest potential methane seepage.

In gas hydrate geological systems, methane leakage events are intermittent and occur in multiple stages, corresponding to changes

TABLE 3 TOC values of cores CL4 and CL40.

Sample	Depth (m)	TOC (wt, %)	Sample	Depth (m)	TOC (wt, %)
CL4-1	0.6	0.76	CL40-1	0.6	0.74
CL4-2	1.2	0.73	CL40-2	1.2	0.76
CL4-3	1.8	0.71	CL40-3	1.8	0.74
CL4-4	2.4	0.72	CL40-4	2.4	0.65
CL4-5	3	0.61	CL40-5	3	0.79
CL4-6	3.6	0.64	CL40-6	3.6	0.73
CL4-7	4.2	0.76	CL40-7	4.2	0.66
CL4-8	4.8	0.68	CL40-8	4.8	0.71

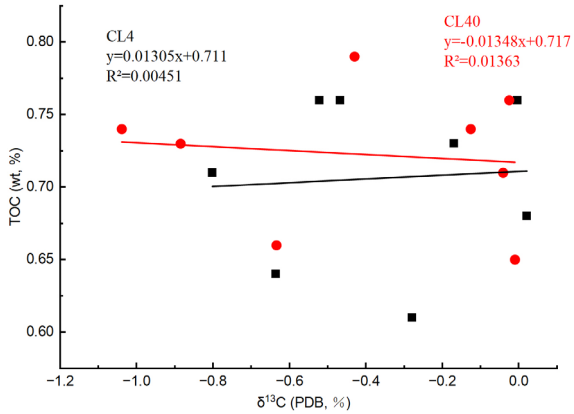

FIGURE 6
Correlation diagram between benthic foraminiferal $\delta^{13}C$ and sediment TOC content at CL4 and CL40 cores. Red represents *C. wuellerstorfi* from site CL40, while black represents *C. wuellerstorfi* from site CL4.

in the stability of gas hydrates. Thus, the negative shift in $\delta^{13}C$ of benthic foraminifera not only reflects the impact of methane leakage but may also be influenced by $\delta^{13}C$ of dissolved inorganic carbon (DIC) in pore water. When organic matter settles to the seafloor, it undergoes anaerobic oxidation under low-oxygen conditions (Equation 3) and aerobic oxidation in an oxic environment (Equation 4). The $\delta^{13}C$ of organic matter is typically around -20‰, and lighter carbon can enter the pore water DIC pool through degradation, leading to a negative shift in $\delta^{13}C$ of benthic foraminifera (Schmiedl and Mackensen, 2006; Kuhnt et al., 2008).

To determine whether enhanced organic matter supply is a primary factor for the negative shift in $\delta^{13}C$, we conducted a series of correlation analyses between sediment total organic carbon (TOC) content and $\delta^{13}C$ of benthic foraminifera. The results showed a very weak correlation between the foraminifera *Cibicidoides wuellerstorfi* and sediment TOC content (Figure 6), indicating that increased organic matter supply is not the dominant factor influencing the negative shift in $\delta^{13}C$ of benthic foraminifera.

$$2CH_2O + SO_4^{2-} \rightarrow 2HCO_3^- + H_2S \quad (3)$$

$$CH_2O + O_2 \rightarrow CO_2 + H_2O \quad (4)$$

In addition to organic matter, methane is another potential source of light carbon. Methane has a very negative $\delta^{13}C$ composition (−110‰ to −30‰). This methane, which is rich in ^{12}C, is converted to HCO_3^- through anaerobic oxidation of methane (AOM) and added to the pore water DIC pool, leading to a significant negative shift in the $\delta^{13}C$ of the pore water DIC. The lowest $\delta^{13}C$ value observed at CL4 was -1.039‰ and at CL40 was -0.802‰, which is significantly lower than fluctuations caused by climate change (<0.6‰) (Wei et al., 2006). This indicates that the strong negative carbon isotope deviation is likely due to the release of highly negative dissolved inorganic carbon from the anaerobic oxidation of methane (AOM). This is consistent with sulfate depletion in the pore water at site QH-CL40 (Figure 5), indicating weak methane seepage, or "micro-seepage" (Wei et al., 2019; Feng et al., 2018a). The variations in carbon isotope depletion reflect changes in methane flux during different seepage stages. Notably, heavier negative $\delta^{13}C$ values at depths of 1.8m and 3-4.2m indicate increased methane seepage activity near the W07 pockmark area of the Qiongdongnan Basin since MIS2 (Rathburn et al., 2003; Bernhard et al., 2010).

Additionally, scanning electron microscopy (SEM) observation of *C. wuellerstorfi* from different layers at sites QH-CL4 and QH-CL40 revealed that foraminifera in layers exhibiting severe $\delta^{13}C$ depletion possessed internal structures encrusted with authigenic carbonate particles (Figure 7). In contrast, foraminifera from layers with minor $\delta^{13}C$ depletion displayed clear, sharp shell edges and open surface pores, indicating no alteration by later authigenic carbonate. The $\delta^{13}C$ anomalies are likely attributed to the formation of secondary carbonate resulting from anaerobic oxidation of methane (AOM).

Moreover, the $\delta^{18}O$ values at these sites show significant positive deviations. At site QH-CL4, the average $\delta^{18}O$ value was 2.63‰, while it was 2.66‰ at site QH-CL40, which both are significantly different from the background values of 0.89‰ to 1.16‰ during the MIS2 period in the South China Sea (Jian, 1998). This suggests the influence of methane seepage activities.

5.2 Methane events recognized and their mechanisms

The carbon and oxygen isotopic data from benthic foraminifera in the Qiongdongnan Basin have revealed two significant anomalies, suggesting major episodes of gas hydrate dissociation and methane release since MIS2 (Figure 3). Globally, methane hydrates on the upper continental slopes are estimated to contain approximately 60 Gt C and are significantly more susceptible to climate-driven changes in bottom water pressure and temperature conditions compared to those found in the deep ocean. Gas hydrates form under low-temperature, high-pressure seabed conditions and are sensitive to external changes in temperature and pressure. Research indicates that sea level fluctuations during

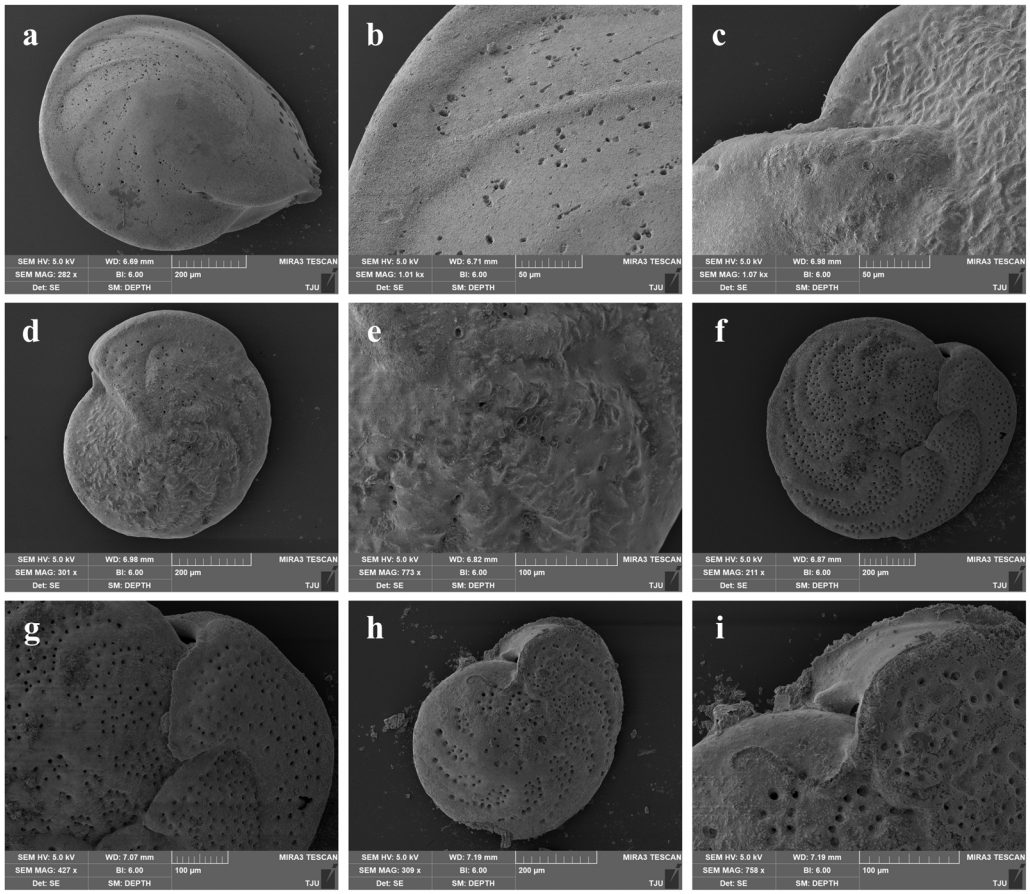

FIGURE 7
Scanning Electron Microscope (SEM) images of the benthic foraminifera *C. weullerstorfi* of the sites QH-CL4 and QH-CL40. **(A, B)** are photos of benthic foraminifera with a relatively slight bias, taken from the QH-CL40 site at a depth of 2.4 meters. Their shells are relatively well-preserved, with open micropores on the surface. **(C-I)** are photos of sections with severe bias in $\delta^{13}C$, showing distinct framboidal pyrite and authigenic carbonate particle accretion.

glacial-interglacial cycles are the primary driver of gas hydrate dissociation, with sea level drops reducing pressure and triggering methane seepage globally (Watanabe et al., 2008; Feng et al., 2018b). Since MIS2, sea levels and seawater temperatures in the South China Sea have changed many times, altering seabed conditions and causing multiple methane seepage events (Dai and Weng, 2015; Yang et al., 2020). Additionally, volcanic activity, and turbidity currents can also trigger methane seepage (Panieri et al., 2014; Bayon et al., 2015; Feng et al., 2015; Liang et al., 2017; Karstens et al., 2018). Understanding the distinction between primary and secondary influences on methane seepage is crucial for comprehending the dynamics of methane release. This paper will explore two significant methane seepage events in the Qiongdongnan Basin as illustrative examples.

5.2.1 Stage 1 (around 19.64-23.22 ka)

Around 19.64~23.22 ka ago, benthic foraminifera carbon isotopes showed a negative excursion, coupled with a positive excursion in oxygen isotopes, indicating an intensification of methane seepage during this period. This corresponds to the Last Glacial Maximum (LGM, approximately 23–18 ka BP). The dissociation of methane hydrates on the South China Sea slope during the LGM is widely documented by various authors (Hu et al., 2017; Li et al., 2017b; Zhang et al., 2018; Liu et al., 2020; Di et al., 2021; Feng et al., 2021; Li et al., 2021, 2023; Dan et al., 2023). During this time, sea levels in the South China Sea dropped by approximately 120 meters compared to present levels (Wang et al., 2020). This sea-level drop led to a reduction in hydrostatic pressure of approximately 1 MPa on the seafloor, destabilizing methane hydrates and increasing methane seepage activity (Rothwell et al., 1998; Holbrook et al., 2002).

Additionally, the lower sea level shortened the distance between river mouths and marginal sea basins, increasing terrestrial sediment supply to the continental slope. This sediment accumulation may have triggered submarine landslides, further promoting gas hydrate dissociation (Kvenvolden, 1993; Zheng et al., 2017). The high sedimentation rate recorded at this layer (~45 cm/ka) supports this interpretation (Table 1).

Therefore, this study concludes that the primary factor driving the intensification of methane seepage during the LGM was the drop in sea level, with increased sedimentation rates due to sea-level changes acting as a secondary factor.

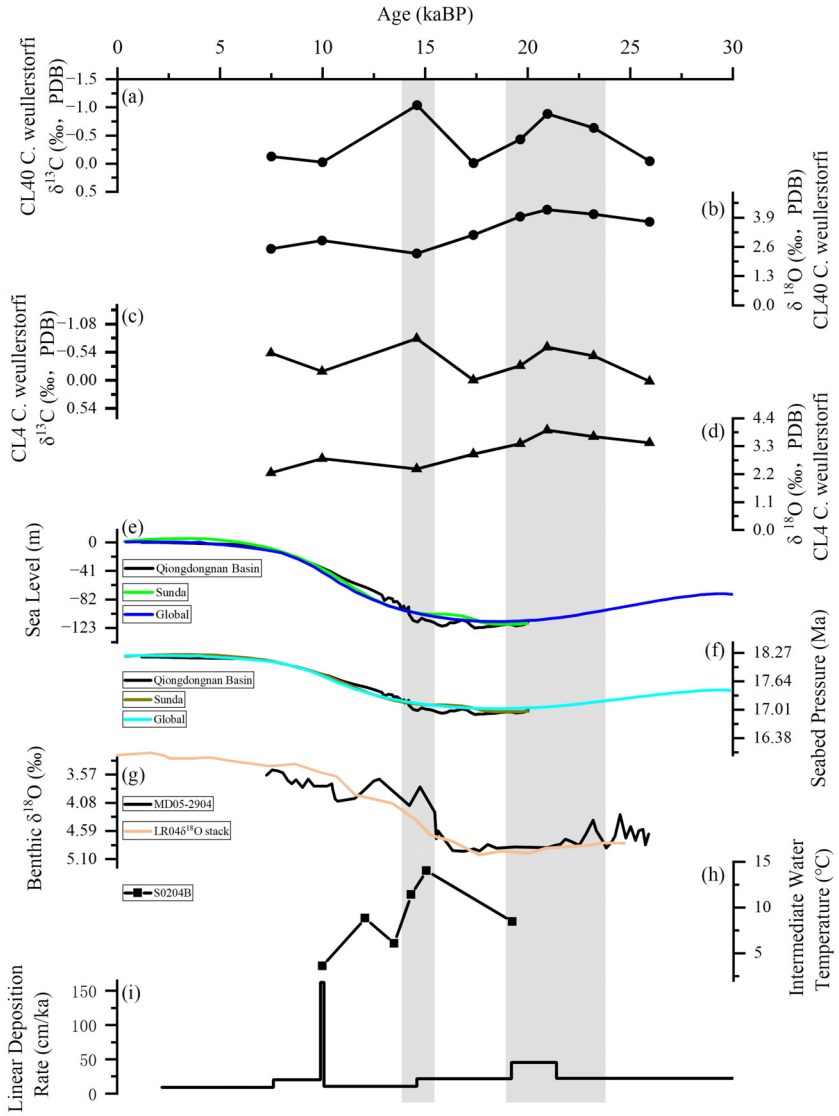

FIGURE 8
Comparison of methane seepage events and control factors. **(A-D)** show the benthic $\delta^{18}O$ and $\delta^{13}C$ measured on *C. wuellerstorfi* at sites QH-CL4 and QH-CL40. **(E)** presents sea-level reconstruction results from Qiongdongnan Basin (Wang et al., 2020), Sunda (Zhao et al., 2017) and the Global mean (Waelbroeck et al., 2002). **(F)** displays the Seabed Pressure calculated based on sea-level changes. **(G)** shows the benthic foraminifera $\delta^{18}O$ of core MD05-2904 (Wan and Jian, 2014) and the LR04 stack (Lisiecki and Raymo, 2005). **(H)** displays the Intermediate water temperature calculated using Mg/Ca ratios of *Globorotalia scitula* (Yang et al., 2020). **(I)** illustrates the Linerar Deposition Rates in Qiongdongnan Basin, as detailed in Table 2.The shaded areas in the figure represent possible stages of enhanced methane seepage.

5.2.2 Stage 2 (around 14.6 ka)

Around 14.6 ka, another increase in methane seepage occurred in the Qiongdongnan Basin. This period marks the end of the Oldest Dryas and the start of the Bølling–Allerød interstadial. However, during this period, both sea level and sea temperature in the Qiongdongnan Basin experienced varying degrees of change (Figure 8). Therefore, identifying the primary and secondary controlling factors is of significant importance.

Compared to the Last Glacial Maximum (LGM), the sea level in the Qiongdongnan Basin has risen by approximately 8.2 meters, resulting in a pressure increase of about 0.08 MPa (Wang et al., 2020). While this rise in sea level has enhanced the stability of seafloor gas hydrates, preventing their dissociation, the overall sea level has remained relatively low since the LGM. Studies show that gas hydrates are more sensitive to changes in bottom water temperature than to hydrostatic pressure (Guan et al., 2022).

During the Bølling–Allerød interstadial, the intermediate water temperature in the South China Sea increased by 6°C (Yang et al., 2020). This rise in oceanic water temperature elevated the bottom water temperature on the continental slope, triggering large-scale dissociation of gas hydrates (Kennett et al., 2000; Camoin and Webster, 2014; Li et al., 2023b). Although increased pressure aids in stabilizing hydrates, the rise in temperature significantly reduces their stability. Research indicates that even a 1°C increase in bottom water temperature can trigger the dissociation of local hydrates, particularly those in shallow sediments (Mienert et al., 2005; Reagan and Moridis, 2007; Westbrook

et al., 2009; Biastoch et al., 2011). During rapid warming events in interglacial periods, temperature increases can negate the stabilizing effect of pressure, leading to hydrate dissociation (Wei et al., 2022).

Therefore, this study identifies the primary driver of enhanced methane seepage during this period as the rise in seawater temperature, with sea level changes as a secondary factor. The variations in sea level and seawater temperature disrupt the thermodynamic equilibrium of hydrates, causing them to dissociate from their stability zone. This process releases large amounts of freshwater and methane gas, which spread into near-seafloor sediments as plumes. These plumes can trigger submarine landslides, leading to turbidity currents that carry large sediment blocks down steep slopes into the deep sea. As a result, fine materials suspended in the water settle over coarser grains, disrupting the original sediment sequence within a certain depth range (Wang et al., 2020).

5.2.3 Correlation between carbon and oxygen isotopes

A negative correlation between carbon and oxygen isotopes was observed at both sites (Figure 3). Notably, during the transition into the Bølling–Allerød interstadial, the carbon isotope at site CL40 dropped to -1.039‰, while at site CL4, it dropped to -0.802‰. However, both sites showed a downward trend in oxygen isotopes, indicating a positive correlation pattern.

Upon further literature review, we found that methane seepage activity generally results in a negative excursion in $\delta^{13}C$ values and a positive excursion in $\delta^{18}O$ values, indicating opposite trends. However, at peripheral seep sites such as GC26 on the Vestnesa Ridge and U1446 in the Mahanadi offshore basin (Panieri et al., 2014; Clemens et al., 2023), carbon isotopes documents strongly negative benthic $\delta^{13}C$ values without significant changes in oxygen isotopes. Moreover, at hydrocarbon-bearing areas like MD2707 site in the Gulf of Guinea and 08CF7 site in the northern South China Sea, benthic foraminifera species such as *C. wuellerstorfi*, *G. crassaformis* and *Uvigerina peregrina* exhibit a positive correlation between $\delta^{13}C$ and $\delta^{18}O$ (Wang et al., 2013; Weldeab et al., 2022). This phenomenon likely results from the combined effects of increased temperatures and changes in bottom water $\delta^{18}O$. Increasing sea water temperature lessens the difference in reaction rates of oxygen isotopes in foraminifera, leading to a reduction in $\delta^{18}O$ (Urey, 1948; Pearson, 2012), attenuating the signal of oxygen isotopes enriched through hydrate decomposition. Consequently, assessments of methane seepage should primarily focus on carbon isotopes.

In this study, at certain depths of the CL4 and CL40 cores, a positive correlation between these isotopes is observed, similar to findings at GC26, indicating that the increase in bottom water temperatures (Figure 8) overshadowed the influence of gas hydrates on the oxygen isotopes. Thus, carbon isotopes in foraminifera reliably record methane seepage activities in the study area.

5.3 Current methane seepage activity indicated by pore water characteristics

At site QH-CL40, sulfate concentrations in pore water decrease continuously from 30.4 mmol/L at 0.6m depth to 19.24 mmol/L at 4.8m depth, indicating ongoing biogeochemical processes consuming sulfate. This depletion is typically associated with two processes: anaerobic oxidation of methane (AOM) and organoclastic sulfate reduction (OSR). AOM occurs when methane interacts with sulfate in the presence of methane-oxidizing bacteria, leading to sulfate depletion at the sulfate-methane interface (SMI) (Borowski et al., 1999). OSR involves sulfate reacting with organic matter in sediments. To determine the primary cause of sulfate depletion, it is essential to assess the contributions of AOM and OSR.

AOM generally has a higher sulfate consumption rate than OSR, characterized by a steep, nearly linear gradient, whereas OSR shows a convex curve (Dickens, 2001; Borowski et al., 1996; Niewöhner et al., 1998; Joye et al., 2004). The sulfate concentration profile at QH-CL40 (Figure 5) shows a steep, nearly linear decline below 1.2m, indicative of strong AOM activity and significant methane seepage. Notably, as sulfate concentrations decrease, Ca^{2+} also decreases with depth, suggesting that bicarbonate produced by AOM increases alkalinity, promoting authigenic carbonate precipitation.

Utilizing Fick's first law, the methane flux at QH-CL40 is calculated to be 28.968 $mmol{\cdot}m^{-2}{\cdot}a^{-1}$, with the sulfate-methane interface (SMI) estimated at a depth of 8.54 m. This site shows a higher methane flux and a shallower SMI compared to other locations in the Qiongdongnan Basin (Table 4). According to global gas hydrate exploration results, areas where SMI <50m and methane flux >3.5 $mmol{\cdot}m^{-2}{\cdot}a^{-1}$ are likely to contain gas hydrates. The SMI depth at QH-CL40 is much less than 50m, thereby validating the potential presence of gas hydrates and suggesting that they may be distributed at shallow depths or even directly exposed on the seabed (Liang et al., 2017; Snyder et al., 2020). In contrast, site QH-CL4 does not exhibit significant sulfate depletion, likely due to fluid dilution or varying seepage intensities within the pockmark area (Hovland et al., 2002; Newman et al., 2008). Consequently, methane flux was not calculated for QH-CL4.

5.4 Controlling factors of current methane leakage

Methane seepage refers to the release of methane from the shallow lithosphere into the hydrosphere and atmosphere (Yang et al., 2021). Some instances of seabed methane seepage are associated with gas hydrate systems, while others originate from deeper gas reservoirs. However, numerous studies have demonstrated that methane seepage in the Qiongdongnan Basin is largely controlled by the presence of gas hydrates within the shallow sediment column (Wang et al., 2018; Wei et al., 2019; Liu et al., 2020; Miao et al., 2021). There is substantial evidence indicating that the Qiongdongnan Basin contains rich gas hydrate resources. Gas hydrates remain stable under low-temperature and high-pressure conditions, so any factors that disrupt these conditions are key to controlling modern methane seepage.

As discussed in section 5.2, we first considers global environmental changes, such as climate shifts, sea level fluctuations, volcanic activity, and tectonic movements, as

TABLE 4 The SMI depth and methane flux of pore water at stations with natural gas hydrate occurrences in the Qiongdongnan Basin.

Site	SMI depth (m)	Methane flux (mmol m^{-2} a^{-1})	Sea water depth (m)	Data source
CL30-2014	5.4	38.9	1255	(Feng et al., 2019)
CL44-2014	7.34	30.9	1279	(Feng et al., 2019)
CL47-2014	7.42	29.0	1301	(Feng et al., 2019)
W08C	9.04	20.6	1737	(Feng et al., 2020)
W09	9.21	24.4	1722	(Feng et al., 2020)
R7	9.05	18.1	1737	(Feng et al., 2020)
R7-1	2.12	76.4	1737	(Feng et al., 2020)
R7-3	3.08	54.1	1737	(Feng et al., 2020)
CL48	111.19	1.6	1722	(Feng et al., 2020)
R1	1.41	159.3	1370	(Hu et al., 2019)
QDN50-15	21.71	9.1	700~2000	(Zhang et al., 2019b)
QDN44-15	18.72	10.7	700~2000	(Zhang et al., 2019b)
QDN14A-15	3.56	94.2	1370	(Hu et al., 2019)
QDN14B-15	4.92	44.7	1370	(Hu et al., 2019)
QDN-C-S03	10.55	18.2	1390~1400	(Hu et al., 2021)
ROV05-CS01	0.33	705.8	1350~1450	(Hu et al., 2021)
R0V01-PC01	2.45	218.7	1400	(Hu et al., 2021)
R0V02-PC01	2.06	108.5	1400	(Jin et al., 2022)
R0V04-PC01	4.56	84.5	1300~1400	(Jin et al., 2022)
QH-CL40	8.54	28.968	1766	This study

potential external influences. However, since 7.5 ka BP, the sedimentation rate at site W7 in the Qiongdongnan Basin has shown no significant changes (Figure 7), which may suggest the absence of substantial turbidite activity. Additionally, foraminifera have not recorded modern methane seepage, making it difficult to confirm whether long-term climate factors have played a significant role in gas hydrate dissociation. Further analysis of sediment grain size data is needed to clarify this relationship.

Another possibility is that methane seepage activity was intensified due to drilling and sampling operations. Hydrate-bearing sediments may destabilize naturally as part of geological processes or during petroleum drilling and production operations (Briaud and Chaouch, 1997). Such drilling activities could disrupt gas hydrates beneath the stable sediment layer, leading to large-scale methane leakage. The dissociation of gas hydrates in the underlying stable zone releases a significant amount of methane into the shallow sediments, resulting in notable anaerobic oxidation of methane (AOM) reactions with sulfate ions in the pore water (Figure 5). This process leads to a rapid depletion of sulfate ions.

Additionally, short-term dynamic changes within the gas hydrate system of the gas chimney may play a significant role in controlling modern methane leakage. As previously mentioned, methane seepage in the Qiongdongnan Basin is influenced by the gas hydrate system. The GMGS5-W7-2018 site is situated above a large gas chimney, where a thick, stable gas hydrate zone is developed. Wei et al. (2019) suggest that this area experiences dynamic changes on a monthly timescale. (1) Fluids migrate vertically through fractures and faults, forming gas hydrates under suitable temperature and pressure conditions. (2) The formation of gas hydrates reduces the permeability of sediments, which in turn decreases the intensity of methane leakage. When fluid migration pathways in fractures become blocked due to insufficient methane supply, the gas hydrates begin to dissolve. (3) As deep pressure accumulates to a certain level, overcoming the rock's hydrostatic pressure, fractures reopen, allowing methane leakage activities to resume (Bangs et al., 2011). This cyclical pressure mechanism regulates the intensity of fluid flow, which ultimately influences the strength of modern methane leakage activities.

5.5 Gas hydrate occurrence inferred from dissolved Cl^- concentrations

Pore water in sediments typically reflects seawater composition, with chloride concentrations approximately 556 mmol/L (Staudigel et al., 1998). At site QH-CL4, chloride levels exhibit a significant decline between 1.8m and 3.6m, reaching a low of 121 mmol/L. This

change is likely attributable to clay mineral dehydration or gas hydrate dissociation (Kim et al., 2013; Kastner, 1991; Torres et al., 2004; Teichert et al., 2005; Kim et al., 2022).

Gas hydrates form under low-temperature, high-pressure conditions, increasing local pore water salinity. However, hydrate dissociation during drilling can lead to reductions in salinity, as observed globally (Huang et al., 2022; Bohrmann et al., 2023; Ye et al., 2019; Torres et al., 2004). The salinity reduction at QH-CL4 aligns with these global patterns, suggesting the presence and dissociation of gas hydrates.

In regions with geothermal gradients above 60°C/km, montmorillonite dehydrates to illite, releasing freshwater and diluting ion concentrations (Dählmann and de Lange, 2003). This process, observed in various locations (Brown et al., 2001; Aloisi et al., 2004; You et al., 2004), typically involves sodium enrichment and potassium depletion in pore water (Huang et al., 2015), which is not evident at QH-CL4. At the QH-CL4 site, the trends of pore water chloride (Cl^-), potassium (K^+), and sodium (Na^+) in the sediment show similar patterns, aligning with the seawater dilution line (Figures 9A, B). Additionally, K^+ and Na^+ exhibit a strong correlation (Figure 9C). Seismic profiles indicate that sites QH-CL4 and QH-CL40 are located in gas chimney structures (Wei et al., 2021), making clay mineral dehydration unlikely, as this process typically occurs in mud volcano zones. Furthermore, clay mineral dehydration releases significant freshwater, affecting larger depth ranges and causing overall concentration reductions, unlike the localized concentration jumps observed in Figure 4 (Bohrmann et al., 2023). Opal dehydration, typically occurring within geothermal gradients of 22-68°C (Murray et al., 1992), is unlikely at these sites due to the higher gradient of approximately 103°C (Wei et al., 2019). Additionally, the shallow depth of the negative chloride anomaly at QH-CL4 suggests minimal diagenetic compaction and pore water migration. This indicates that the pore water concentration at QH-CL4 is more consistent with gas hydrate dissociation than with clay mineral dehydration or diagenetic compaction. Therefore, the 1.8m to 3.6m depth range at QH-CL4 likely contains gas hydrates that dissociate during core recovery, releasing freshwater and methane, which causes the observed chloride concentration anomaly (Figure 3).

5.6 Mechanisms behind the rapid formation of gas hydrates in shallow sediments

In the Qiongdongnan Basin, gas hydrates typically occur between 6m and 250m below the seabed, situated near the gas hydrate stability zone. LWD Resistivity indicate that the upper boundary of this stability zone is located at a depth of 22.5m (Wei et al., 2019). However, analyses of pore water salinity and sulfate concentrations indicate the presence of gas hydrates in very shallow sediments (0-5m), suggesting localized hydrate mounds.

Recent studies on the dynamics of gas hydrate formation in methane seep areas have addressed this concern (Zhang et al., 2023b; Wang et al., 2024; Xie et al., 2024; Zhang et al., 2024). These studies indicate that near the seabed at methane seep outlets, the induction time for gas hydrate formation, influenced by memory effects and authigenic carbonate particles, is less than two minutes, with a metastable nucleation time of only ten seconds. This provides a theoretical basis for the occurrence of shallow gas hydrates.

Fluid properties, gas origins, solid particle types, and the hydrate memory effect significantly influence gas hydrate formation (Zhang et al., 2023b). In fluid seep environments, hydrate formation requires less induction time compared to freshwater and seawater environments due to the inhibitory effects of chloride ions present in seawater. Freshwater released from decomposing bottom hydrates dilutes the surrounding fluid, resulting in salinity levels that fall below those of seawater.

Additionally, carbonate particles accelerate hydrate formation by increasing the contact area between gas and liquid phases. Ion concentration analyses show declining calcium levels with depth (Figure 4), indicating the likely presence of authigenic carbonate particles. SEM analysis of foraminifera shells reveals attached carbonate particles (Figure 6), supporting this hypothesis and providing evidence for rapid gas hydrate formation.

Furthermore, research shows that gas bubbles from melted hydrates form gas hydrates more readily than primary methane bubbles, a phenomenon referred to as the hydrate memory effect (Uchida et al., 2000; Lee et al., 2005). In the Qiongdongnan Basin,

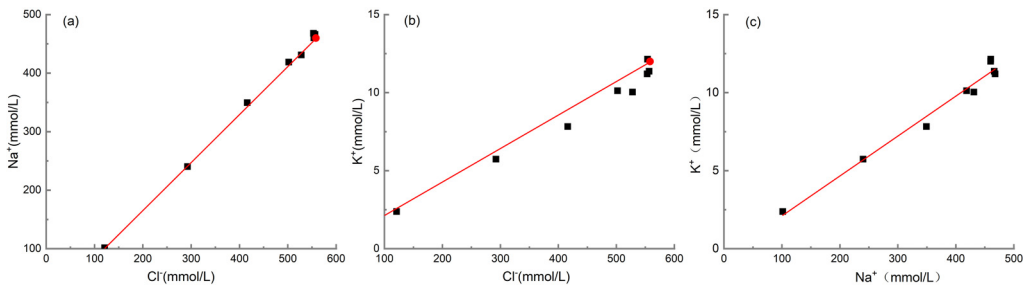

FIGURE 9
Correlation graph of pore water concentrations between Na^+ and Cl^- **(A)**, K^+ and Cl^- **(B)**, K^+ and Na^+ **(C)** in the QH-CL4 columnar sediments. The red dots in graphs **(A, B)** indicate the concentrations of Na^+, K^+, and Cl^- in seawater, while the black squares represent the actual measured values. The solid red lines in these graphs depict the seawater dilution line. Additionally, in graph **(C)**, the solid red line signifies the fitted curve for the concentrations of K^+ and Na^+.

gas hydrates located near the stability zone are prone to temperature and pressure changes, leading to their dissociation. The released methane bubbles ascend rapidly along gas chimneys, aggregating with authigenic carbonate nodules at seepage exits, where the memory effect facilitates accelerated hydrate formation. Dilution by seepage fluid further enhances this process.

In conclusion, ongoing methane seepage in the Qiongdongnan Basin has led to the formation of gas hydrates in near-seabed shallow sediments. Fluid properties, thermogenic methane, authigenic carbonate nodules, and the hydrate memory effect collectively contribute to the formation of these shallow gas hydrates.

6 Conclusion

Analysis of foraminifera stable isotopes and pore water geochemistry at sites QH-CL4 and QH-CL40 reveals persistent methane microseepage in the Qiongdongnan Basin since MIS2. Significant carbon isotope depletion at 1.8m and 3m indicates increased seepage around 14.6ka and 19.64ka, possibly associated with sea-level drops during the Last Glacial Maximum and rising temperatures during the Bølling–Allerød interstadial. QH-CL40 has an SMI depth of 8.54m and a methane flux of 28.968mmol×m^{-2}×a^{-1}, suggesting strong potential for hydrate development. Severe salinity reduction between 1.8m and 3.6m at QH-CL4 indicates shallow gas hydrate formation, accelerated by both the hydrate memory effect and authigenic carbonate particles.

Data availability statement

The original contributions presented in the study are included in the article/supplementary material. Further inquiries can be directed to the corresponding author.

Ethics statement

The manuscript presents research on animals that do not require ethical approval for their study.

Author contributions

XL: Conceptualization, Data curation, Formal analysis, Methodology, Software, Writing – original draft. YY: Conceptualization, Data curation, Formal analysis, Funding acquisition, Methodology, Project administration, Software, Supervision, Validation, Writing – original draft, Writing – review & editing. WZ: Conceptualization, Data curation, Funding acquisition, Investigation, Resources, Software, Supervision, Writing – original draft, Writing – review & editing. WH: Investigation, Writing – review & editing. SO: Formal analysis, Visualization, Writing – original draft, Writing – review & editing. CJ: Investigation, Writing – review & editing. JC: Investigation, Writing – review & editing.

Funding

The author(s) declare that financial support was received for the research, authorship, and/or publication of this article. This study was supported by National Natural Science Foundation of China (42102256, 42230705 and 42176215), National Engineering Research Center of Gas Hydrate Exploration and Development (NERCY(202407) and NERCY2024002), Project of Sanya Yazhou Bay Science and Technology City (SCKJ-JYRC-2023-02), First Batch of "Nanhai New Star" project (NHXXRCXM202357), Sanya Science and Technology Inovation Project (2022KJCX14), and the Undergraduate Innovation and Entrepreneurship Training Program of South China Normal University. The Guangzhou Basic and Applied Basic Research Foundation (Grant No. 202201011106).

Acknowledgments

Thank to those who contributed to the success of the fifth gas hydrate drilling expedition (GMGS5). Thanks Bigyan Neupane for his significant contribution to the language refinement of this paper.

Conflict of interest

The authors declare that the research was conducted in the absence of any commercial or financial relationships that could be construed as a potential conflict of interest.

Publisher's note

References

Aloisi, G., Drews, M., Wallmann, K., and Bohrmann, G. (2004). Fluid expulsion from the dvurechenskii mud volcano (black sea): Part I. Fluid sources and relevance to li, B, sr, I and dissolved inorganic nitrogen cycles. *Earth Planet. Sci. Lett.* 225, 347–363. doi: 10.1016/j.epsl.2004.07.006

Archer, D., Buffett, B., and Brovkin, V. (2009). Ocean methane hydrates as a slow tipping point in the global carbon cycle. *Proc. Natl. Acad. Sci.* 106, 20596–20601. doi: 10.1073/pnas.0800885105

Bangs, N. L. B., Hornbach, M. J., and Berndt, C. (2011). The mechanics of intermittent methane venting at south hydrate ridge inferred from 4D seismic surveying. *Earth Planet. Sci. Lett.* 310, 105–112. doi: 10.1016/j.epsl.2011.06.022

Bayon, G., Henderson, G. M., Etoubleau, J., Caprais, J.-C., Ruffine, L., Marsset, T., et al. (2015). U-th isotope constraints on gas hydrate and pockmark dynamics at the Niger delta margin. *Mar. Geol.* 370, 87–98. doi: 10.1016/j.margeo.2015.10.012

Bernhard, J. M., Martin, J. B., and Rathburn, A. E. (2010). Combined carbonate carbon isotopic and cellular ultrastructural studies of individual benthic foraminifera: 2. Toward an understanding of apparent disequilibrium in hydrocarbon seeps. *Paleoceanography* 25, PA4206. doi: 10.1029/2010PA001930

Biastoch, A., Treude, T., Rüpke, L. H., Riebesell, U., Roth, C., Burwicz, E. B., et al (2011). Rising arctic ocean temperatures cause gas hydrate destabilization and ocean acidification. *Geophysical Research Letters* 38, L08602. doi: 10.1029/2011GL047222

Boetius, A., and Wenzhoefer, F. (2013). Boetius a, wenzh??fer F. Seafloor oxygen consumption fuelled by methane from cold seeps. Nat geosci 6: 725-734. *Nat. Geosci.* 6, 725–734. doi: 10.1038/ngeo1926

Bohrmann, G., Berndt, C., Lin, S., Tu, T.-H., Lin, A. T., Hsu, H.-H., et al. (2023). Geological controls on the distribution of gas hydrates in the shallow parts of the gas hydrate stability zone – constraints from seafloor drilling off Taiwan. *Mar. Pet. Geol.* 153, 106253. doi: 10.1016/j.marpetgeo.2023.106253

Borowski, W. S., Paull, C. K., and Ussler, W. (1996). Marine pore-water sulfate profiles indicate in *situ* methane flux from underlying gas hydrate. *Geology* 24, 655. doi: 10.1130/0091-7613(1996)024<0655:MPWSPI>2.3.CO;2

Borowski, W. S., Paull, C. K., and Ussler, W. (1999). Global and local variations of interstitial sulfate gradients in deep-water, continental margin sediments: Sensitivity to underlying methane and gas hydrates. *Mar. Geol.* 159, 131–154. doi: 10.1016/S0025-3227(99)00004-3

Briaud, J.-L., and Chaouch, A. (1997). Hydrate melting in soil around hot conductor. *J. Geotech. Geoenvironmental Eng.* 123, 645–653. doi: 10.1061/(ASCE)1090-0241(1997)123:7(645

Brown, K. M., Saffer, D. M., and Bekins, B. A. (2001). Smectite diagenesis, pore-water freshening, and fluid flow at the toe of the nankai wedge. *Earth Planet. Sci. Lett.* 194, 97–109. doi: 10.1016/S0012-821X(01)00546-5

Burkett, A. M., Rathburn, A. E., Pérez, M. E., and Martin, J. B. (2018). Influences of thermal and fluid characteristics of methane and hydrothermal seeps on the stable oxygen isotopes of living benthic foraminifera. *Mar. Pet. Geol.* 93, 344–355. doi: 10.1016/j.marpetgeo.2018.02.037

Camoin, G., and Webster, J. (2014). "Chapter 3.6 - coral reefs and sea-level change," in *Developments in Marine Geology*. Eds. R. Stein, D. K. Blackman, F. Inagaki and H.-C. Larsen (Amsterdam/New York: Elsevier), 395–441. doi: 10.1016/B978-0-444-62617-2.00015-3

Cen, Y., Wang, J., Ding, X., Stow, D., Wang, Z., Chen, C., et al. (2022). Tracing the methane events by stable carbon isotopes of benthic foraminifera at glacial periods in the andaman sea. *J. Earth Sci.* 33, 1571–1582. doi: 10.1007/s12583-022-1750-x

Cheng, X., Wang, P., Huang, B., Liu, C., Jian, Z., Zhao, Q., et al. (2005). Carbon isotopic study of foraminiferal tests in surface sediments of the South China Sea and its significance. *Sci. Bull.* (50), 162–166. doi: 10.1007/BF02897520

Clemens, S. C., Thirumalai, K., and Oppo, D. (2023). Indian margin methane hydrate dissociation recorded in the carbon isotopes of benthic (miliolida) foraminifera. *Earth Planet. Sci. Lett.* 609, 118101. doi: 10.1016/j.epsl.2023.118101

Dählmann, A., and de Lange, G. J. (2003). Fluid–sediment interactions at eastern mediterranean mud volcanoes: A stable isotope study from ODP leg 160. *Earth Planet. Sci. Lett.* 212, 377–391. doi: 10.1016/S0012-821X(03)00227-9

Dai, L., and Weng, C. (2015). Marine palynological record for tropical climate variations since the late last glacial maximum in the northern south China sea. *Deep. Sea. Res. Part II. Top. Stud. Oceanogr.* 122, 153–162. doi: 10.1016/j.dsr2.2015.06.011

Dan, X., Liu, S., Feng, X., Lin, L., Tang, R., Yang, C., et al. (2023). Geochemical record of methane seepage in carbon cycling and possible correlation with climate events in the qiongdongnan basin, south China sea. *Mar. Pet. Geol.* 149, 106061. doi: 10.1016/j.marpetgeo.2022.106061

Deng, W., Liang, J., Kuang, Z., Zhang, W., He, Y., Meng, M., et al. (2021). Permeability prediction for unconsolidated hydrate reservoirs with pore compressibility and porosity inversion in the northern South China Sea. *J. Nat. Gas. Sci. Eng.* 95, 104161. doi: 10.1016/j.jngse.2021.104161

Dessandier, P.-A., Borrelli, C., Yao, H., Sauer, S., Hong, W.-L., and Panieri, G. (2020). Foraminiferal δ18O reveals gas hydrate dissociation in arctic and north atlantic ocean sediments. *Geo-Mar. Lett.* 40, 507–523. doi: 10.1007/s00367-019-00635-6

Di, P., Yang, X., Rashid, H., Zhou, Y., Wang, H., Li, N., et al. (2021). Enhanced sulfidization in a sedimentary turbidite layer from the nansha trough in the southern south China sea. *Sediment. Geol.* 421, 105955. doi: 10.1016/j.sedgeo.2021.105955

Dickens, G. R. (2001). Sulfate profiles and barium fronts in sediment on the blake ridge: Present and past methane fluxes through a large gas hydrate reservoir. *Geochim. Cosmochim. Acta* 65, 529–543. doi: 10.1016/S0016-7037(00)00556-1

Dickens, G. R., Castillo, M. M., and Walker, J. C. G. (1997). A blast of gas in the latest paleocene: Simulating first-order effects of massive dissociation of oceanic methane hydrate. *Geology* 25, 259. doi: 10.1130/0091-7613(1997)025<0259:ABOGIT>2.3.CO;2

Dou, Y., Li, Q., Wu, Y., Zhao, J., Sun, C., Cai, F., et al. (2022). Carbon and oxygen isotopic characteristics of benthic foraminifera in the Okinawa Trough since MIS6 and their palaeoceanographical significance. *Earth Sci. Front.* 29, 084~092. doi: 10.13745/j.esf.sf.2022.1.14

Feng, D., Cheng, M., Kiel, S., Qiu, J.-W., Yang, Q., Zhou, H., et al. (2015). Using bathymodiolus tissue stable carbon, nitrogen and sulfur isotopes to infer biogeochemical process at a cold seep in the south China sea. *Deep. Sea. Res. Part Oceanogr. Res. Pap.* 104, 52–59. doi: 10.1016/j.dsr.2015.06.011

Feng, J., Li, N., Liang, J., Shang, J., Yang, S., and Wang, H. (2021). Using multi-proxy approach to constrain temporal variations of methane flux in methane-rich sediments of the southern south China sea. *Mar. Pet. Geol.* 132, 105152. doi: 10.1016/j.marpetgeo.2021.105152

Feng, J., Li, N., Luo, M., Liang, J., Yang, S., Wang, H., et al. (2020). A quantitative assessment of methane-derived carbon cycling at the cold seeps in the northwestern south China sea. *Minerals* 10, 256. doi: 10.3390/min10030256

Feng, D., Qiu, J.-W., Hu, Y., Peckmann, J., Guan, H., Tong, H., et al. (2018b). Cold seep systems in the south China sea: An overview. *J. Asian Earth Sci.* 168, 3–16. doi: 10.1016/j.jseaes.2018.09.021

Feng, J., Yang, S., Sun, X., and Liang, J. (2018a). Geochemical tracers for methane microleakage activity in the qiongdongnan basin. *J. Southwest. Petreleum. Univ. (Science. Technol. Edition).* 40, 63~75. 10.11885/j.issn.1674-5086.2017.12.01.01

Feng, J., Yang, S., Wang, H., Liang, J., Fang, Y., and Luo, M. (2019). Methane source and turnover in the shallow sediments to the west of haima cold seeps on the northwestern slope of the south China sea. *Geofluids* 2019, 1010824. doi: 10.1155/2019/1010824

Guan, H., Liu, L., Hu, Y., Li, S., Li, N., Sun, Z., et al. (2022). Rising bottom-water temperatures induced methane release during the middle holocene in the okinawa trough, east China sea. *Chem. Geol.* 590, 120707. doi: 10.1016/j.chemgeo.2022.120707

Haeckel, M., Suess, E., Wallmann, K., and Rickert, D. (2004). Rising methane gas bubbles form massive hydrate layers at the seafloor. *Geochim. Cosmochim. Acta* 68, 4335–4345. doi: 10.1016/j.gca.2004.01.018

Hesse, R., and Harrison, W. E. (1981). Gas hydrates (clathrates) causing pore-water freshening and oxygen isotope fractionation in deep-water sedimentary sections of terrigenous continental margins. *Earth Planet. Sci. Lett.* 55, 453–462. doi: 10.1016/0012-821X(81)90172-2

Hill, T. M., Kennett, J. P., and Spero, H. J. (2003). Foraminifera as indicators of methane-rich environments: A study of modern methane seeps in santa barbara channel, california. *Mar. Micropaleontol.* 49, 123–138. doi: 10.1016/S0377-8398(03)00032-X

Hill, T. M., Kennett, J. P., and Valentine, D. L. (2004). Isotopic evidence for the incorporation of methane-derived carbon into foraminifera from modern methane seeps, hydrate ridge, northeast pacific. *Geochim. Cosmochim. Acta* 68, 4619–4627. doi: 10.1016/j.gca.2004.07.012

Holbrook, S., Lizarralde, D., Pecher, I., Gorman, A., Hackwith, K., Hornbach, M., et al. (2002). Escape of methane gas through sediment waves in a large methane hydrate province. *Geology* 30, 467–470. doi: 10.1130/0091-7613(2002)030<0467:EOMGTS>2.0.CO;2

Hong, W.-L., Torres, M. E., Portnov, A., Waage, M., Haley, B., and Lepland, A. (2018). Variations in gas and water pulses at an arctic seep: fluid sources and methane transport. *Geophys. Res. Lett.* 45, 4153–4162. doi: 10.1029/2018GL077309

Hovland, M., Gardner, J. V., and Judd, A. G. (2002). The significance of pockmarks to understanding fluid flow processes and geohazards. *Geofluids* 2, 127–136. doi: 10.1046/j.1468-8123.2002.00028.x

Hu, Y., Chen, L., Feng, D., Liang, Q., Xia, Z., and Chen, D. (2017). Geochemical record of methane seepage in authigenic carbonates and surrounding host sediments: A case study from the south China sea. *J. Asian Earth Sci.* 138, 51–61. doi: 10.1016/j.jseaes.2017.02.004

Hu, Y., Luo, M., Liang, Q., Chen, L., Feng, D., Yang, S., et al. (2019). Pore fluid compositions and inferred fluid flow patterns at the Haima cold seeps of the South China Sea. *Mar. Pet. Geol.* 103, 29–40. doi: 10.1016/j.marpetgeo.2019.01.007

Hu, T., Luo, M., Xu, Y., Gong, S., and Chen, D. (2021). Production of labile protein-like dissolved organic carbon associated with anaerobic methane oxidization in the haima cold seeps, south China sea. *Front. Mar. Sci.* 8. doi: 10.3389/fmars.2021.797084

Hu, B., Wang, L., Yan, W., Liu, S., Cai, D., Zhang, G., et al. (2013). The tectonic evolution of the qiongdongnan basin in the northern margin of the south China sea. *J. Asian Earth Sci.* 77, 163–182. doi: 10.1016/j.jseaes.2013.08.022

Huang, Y., Cheng, J., Wang, M., Wang, S., and Yan, W. (2022). Gas hydrate dissociation events during LGM and their potential trigger of submarine landslides: Foraminifera and geochemical records from two cores in the northern south China sea. *Front. Earth Sci.* 10. doi: 10.3389/feart.2022.876913

Huang, H., Li, N., Wang, Q., and Chen, D. (2015). Geochemical features and origins of pore fluids and sediments of the mud volcanoes in southern margin of the junggar basin, xinjiang, northwestern China. *Geotectonica. Metallogenia.* 39, 325–333. doi: 10.16539/j.ddgzyckx.2015.02.012

Jian, Z. (1998). Stable isotopic records of the glacial deep-water properties in the south China sea. *Sci. China Ser. Earth Sci.* 41, 337–344. doi: 10.1007/BF02932683

Jin, M., Feng, D., Huang, K., Gong, S., Luo, M., Peckmann, J., et al. (2022). Magnesium isotopes in pore water of active methane seeps of the south China sea. *Front. Mar. Sci.* 9. doi: 10.3389/fmars.2022.858860

Joye, S. B., Boetius, A., Orcutt, B. N., Montoya, J. P., Schulz, H. N., Erickson, M. J., et al. (2004). The anaerobic oxidation of methane and sulfate reduction in sediments from gulf of Mexico cold seeps. *Chem. Geol.* 205, 219–238. doi: 10.1016/j.chemgeo.2003.12.019

Karstens, J., Haflidason, H., Becker, L. W. M., Berndt, C., Rüpke, L., Planke, S., et al. (2018). Glacigenic sedimentation pulses triggered post-glacial gas hydrate dissociation. *Nat. Commun.* 9, 635. doi: 10.1038/s41467-018-03043-z

Kastner, M. (1991). Fluids in convergent margins: What do we know about their composition, origin, role in diagenesis and importance for oceanic chemical fluxes? *Philos. Trans. R. Soc Lond. Ser. Phys. Eng. Sci.* 335, 243–259. doi: 10.1098/rsta.1991.0045

Kennett, J. P., Cannariato, K. G., Hendy, I. L., and Behl, R. J. (2000). Carbon isotopic evidence for methane hydrate instability during quaternary interstadials. *Science* 288, 128–133. doi: 10.1126/science.288.5463.128

Kim, J.-H., Park, M.-H., Lee, D.-H., Minami, H., Jin, Y.-K., Hachikubo, A., et al. (2022). Impact of high methane flux on the properties of pore fluid and methane-derived authigenic carbonate in the ARAON mounds, Chukchi sea. *Front. Mar. Sci.* 9. doi: 10.3389/fmars.2022.944841

Kim, J.-H., Torres, M. E., Hong, W.-L., Choi, J., Riedel, M., Bahk, J.-J., et al. (2013). Pore fluid chemistry from the Second Gas Hydrate Drilling Expedition in the Ulleung Basin (UBGH2): Source, mechanisms and consequences of fluid freshening in the central part of the Ulleung Basin, East Sea. *Mar. Pet. Geol.* 47, 99–112. doi: 10.1016/j.marpetgeo.2012.12.011

Kirschke, S., Bousquet, P., Ciais, P., Saunois, M., Canadell, J. G., Dlugokencky, E. J., et al. (2013). Three decades of global methane sources and sinks. *Nat. Geosci.* 6, 813–823. doi: 10.1038/ngeo1955

Kubota, Y., Kimoto, K., Itaki, T., Yokoyama, Y., Miyairi, Y., and Matsuzaki, H. (2015). Bottom water variability in the subtropical northwestern pacific from 26 kyr BP to present based on mg/ca and stable carbon and oxygen isotopes of benthic foraminifera. *Clim. Past.* 11, 803–824. doi: 10.5194/cp-11-803-2015

Kuhnt, T., Schmiedl, G., Ehrmann, W., Hamann, Y., and Andersen, N. (2008). Stable isotopic composition of holocene benthic foraminifers from the eastern mediterranean sea: Past changes in productivity and deep water oxygenation. *Palaeogeogr. Palaeoclimatol. Palaeoecol.* 268, 106–115. doi: 10.1016/j.palaeo.2008.07.010

Kvenvolden, K. A. (1993). Gas hydrates—geological perspective and global change. *Rev. Geophys.* 31, 173–187. doi: 10.1029/93RG00268

Kvenvolden, K. A. (1995). A review of the geochemistry of methane in natural gas hydrate. *Org. Geochem.* 23, 997–1008. doi: 10.1016/0146-6380(96)00002-2

Lai, H., Fang, Y., Kuang, Z., Ren, J., Liang, J., Lu, J., et al. (2021). Geochemistry, origin and accumulation of natural gas hydrates in the Qiongdongnan Basin, South China Sea: Implications from site GMGS5-W08. *Mar. Pet. Geol.* 123, 104774. doi: 10.1016/j.marpetgeo.2020.104774

Lee, J. D., Susilo, R., and Englezos, P. (2005). Kinetics of structure H gas hydrate formation. *Energy Fuels* 19, 1008–1015. doi: 10.1021/ef049729+

Lemaitre, N., Bayon, G., Ondréas, H., Caprais, J.-C., Freslon, N., Bollinger, C., et al. (2014). Trace element behaviour at cold seeps and the potential export of dissolved iron to the ocean. *Earth Planet. Sci. Lett.* 404, 376–388. doi: 10.1016/j.epsl.2014.08.014

Li, N., Feng, D., Chen, L., Wang, H., and Chen, D. (2017b). Compositions of foraminifera-rich turbidite sediments from the shenhu area on the northern slope of the south China sea: Implication for the presence of deep water bottom currents. *J. Asian Earth Sci.* 138, 148–160. doi: 10.1016/j.jseaes.2017.02.010

Li, C., Lv, C., Chen, G., Zhang, G., Ma, M., Shen, H., et al. (2017a). Source and sink characteristics of the continental slope-parallel central canyon in the qiongdongnan basin on the northern margin of the south China sea. *J. Asian Earth Sci.* 134, 1–12. doi: 10.1016/j.jseaes.2016.10.014

Li, J., Miao, X., Feng, X., Jiang, R., Zhao, M., Dan, X., et al. (2023a). Pulsed turbidite and methane seep records in the north western south China sea since the last glacial maximum. *Front. Mar. Sci.* 10. doi: 10.3389/fmars.2023.1147751

Li, N., Wang, X., Feng, J., Chen, F., Zhou, Y., Wang, M., et al. (2023b). Intermediate water warming caused methane hydrate instability in south China sea during past interglacials. *GSA. Bull.* 136, 917–927. doi: 10.1130/B36859.1

Li, N., Yang, X., Peckmann, J., Zhou, Y., Wang, H., Chen, D., et al. (2021). Persistent oxygen depletion of bottom waters caused by methane seepage: Evidence from the south China sea. *Ore. Geol. Rev.* 129, 103949. doi: 10.1016/j.oregeorev.2020.103949

Liang, Q., Hu, Y., Feng, D., Peckmann, J., Chen, L., Yang, S., et al. (2017). Authigenic carbonates from newly discovered active cold seeps on the northwestern slope of the south China sea: Constraints on fluid sources, formation environments, and seepage dynamics. *Deep. Sea. Res. Part Oceanogr. Res. Pap.* 124, 31–41. doi: 10.1016/j.dsr.2017.04.015

Liang, C., Jiang, T., Kuang, Z., Hu, Y., Yang, C., Ren, J., et al. (2024). Sedimentary time and genesis mechanism of natural gas hydrate reservoirs in the Qiongdongnan Basin. *Earth Sci. Front.*, 1–17.

Lisiecki, L. E., and Raymo, M. E. (2005). A pliocene-pleistocene stack of 57 globally distributed benthic δ18O records. *Paleoceanography* 20, PA1003. doi: 10.1029/2004PA001071

Liu, S., Feng, X., Feng, Z., Xiao, X., and Feng, L. (2020). Geochemical evidence of methane seepage in the sediments of the qiongdongnan basin, south China sea. *Chem. Geol.* 543, 119588. doi: 10.1016/j.chemgeo.2020.119588

Mackensen, A., Schmiedl, G., Thiele, J., and Damm, E. (2017). Microhabitat preferences of live benthic foraminifera and stable carbon isotopes off SW svalbard in the presence of widespread methane seepage. *Mar. Micropaleontol.* 132, 1–17. doi: 10.1016/j.marmicro.2017.04.004

Mackensen, A., Wollenburg, J., and Licari, L. (2006). Low δ13C in tests of live epibenthic and endobenthic foraminifera at a site of active methane seepage. *Paleoceanography* 21, PA2022. doi: 10.1029/2005PA001196

Malinverno, A., Kastner, M., Torres, M. E., and Wortmann, U. G. (2008). Gas hydrate occurrence from pore water chlorinity and downhole logs in a transect across the northern Cascadia margin (Integrated Ocean Drilling Program Expedition 311). *J. Geophys. Res. Solid. Earth* 113, B08103. doi: 10.1029/2008JB005702

McCorkle, D. C., Keigwin, L. D., Corliss, B. H., and Emerson, S. R. (1990). The influence of microhabitats on the carbon isotopic composition of deep-sea benthic foraminifera. *Paleoceanography* 5, 161–185. doi: 10.1029/PA005i002p00161

Melaniuk, K., Sztybor, K., Treude, T., Sommer, S., and Rasmussen, T. L. (2022b). Influence of methane seepage on isotopic signatures in living deep-sea benthic foraminifera, 79° N. *Sci. Rep.* 12, 1169. doi: 10.1038/s41598-022-05175-1

Melaniuk, K., Sztybor, K., Treude, T., Sommer, S., Zajączkowski, M., and Rasmussen, T. L. (2022a). Response of benthic foraminifera to environmental successions of cold seeps from vestnesa ridge, svalbard: Implications for interpretations of paleo-seepage environments. *Front. Mar. Sci.* 9. doi: 10.3389/fmars.2022.999902

Miao, X., Feng, X., Li, J., and Lin, L. (2021). Tracing the paleo-methane seepage activity over the past 20,000 years in the sediments of qiongdongnan basin, northwestern south China sea. *Chem. Geol.* 559, 119956. doi: 10.1016/j.chemgeo.2020.119956

Mienert, J., Vanneste, M., Bünz, S., Andreassen, K., Haflidason, H., and Sejrup, H. P. (2005). Ocean warming and gas hydrate stability on the mid-norwegian margin at the storegga slide. *Marine and Petroleum Geology* 22, 233–244. doi: 10.1016/j.marpetgeo.2004.10.018

Murray, R. W., Buchholtz Ten Brink, M. R., Gerlach, D. C., Price Russ, G., and Jones, D. L. (1992). Rare earth, major, and trace element composition of monterey and DSDP chert and associated host sediment: Assessing the influence of chemical fractionation during diagenesis. *Geochim. Cosmochim. Acta* 56, 2657–2671. doi: 10.1016/0016-7037(92)90351-I

Newman, K. R., Cormier, M.-H., Weissel, J. K., Driscoll, N. W., Kastner, M., Solomon, E. A., et al. (2008). Active methane venting observed at giant pockmarks along the U.S. mid-atlantic shelf break. *Earth Planet. Sci. Lett.* 267, 341–352. doi: 10.1016/j.epsl.2007.11.053

Niemann, H., Lösekann, T., De Beer, D., Elvert, M., Nadalig, T., Knittel, K., et al. (2006). Novel microbial communities of the haakon mosby mud volcano and their role as a methane sink. *Nature* 443, 854–858. doi: 10.1038/nature05227

Niewöhner, C., Hensen, C., Kasten, S., Zabel, M., and Schulz, H. D. (1998). Deep sulfate reduction completely mediated by anaerobic methane oxidation in sediments of the upwelling area off Namibia. *Geochim. Cosmochim. Acta* 62, 455–464. doi: 10.1016/S0016-7037(98)00055-6

Panieri, G., James, R. H., Camerlenghi, A., Westbrook, G. K., Consolaro, C., Cacho, I., et al. (2014). Record of methane emissions from the west svalbard continental margin during the last 23.500 yrs revealed by δ13C of benthic foraminifera. *Glob. Planet. Change* 122, 151–160. doi: 10.1016/j.gloplacha.2014.08.014

Pearson, P. N. (2012). Oxygen isotopes in foraminifera: Overview and historical review. *Paleontol. Soc Pap.* 18, 1–38. doi: 10.1017/S1089332600002539

Rathburn, A. E., Levin, L. A., Held, Z., and Lohmann, K. C. (2000). Benthic foraminifera associated with cold methane seeps on the northern california margin: Ecology and stable isotopic composition. *Mar. Micropaleontol.* 38, 247–266. doi: 10.1016/S0377-8398(00)00005-0

Rathburn, A. E., Pérez, M. E., Martin, J. B., Day, S. A., Mahn, C., Gieskes, J., et al. (2003). Relationships between the distribution and stable isotopic composition of living benthic foraminifera and cold methane seep biogeochemistry in monterey bay, california. *Geochem. Geophys. Geosyst.* 4, 1106. doi: 10.1029/2003GC000595

Reagan, M. T., and Moridis, G. J. (2007). Oceanic gas hydrate instability and dissociation under climate change scenarios. *Geophys. Res. Lett.* 34, L22709. doi: 10.1029/2007GL031671

Ren, J., Cheng, C., Xiong, P., Kuang, Z., Liang, J., Lai, H., et al. (2022). Sand-rich gas hydrate and shallow gas systems in the Qiongdongnan Basin, northern South China Sea. *J. Pet. Sci. Eng.* 215, 110630. doi: 10.1016/j.petrol.2022.110630

Rothwell, R. G., Thomson, J., and Kähler, G. (1998). Low-sea-level emplacement of a very large late pleistocene 'megaturbidite' in the western mediterranean sea. *Nature* 392, 377–380. doi: 10.1038/32871

Ryan, W. B. F., Carbotte, S. M., Coplan, J. O., O'Hara, S., Melkonian, A., Arko, R., et al. (2009). Global multi-resolution topography synthesis. *Geochemistry, Geophysics, Geosystems* 10, Q03014. doi: 10.1029/2008GC002332

Scheiner, F., Holcová, K., Milovský, R., and Kuhnert, H. (2018). Temperature and isotopic composition of seawater in the epicontinental sea (central paratethys) during the middle miocene climate transition based on mg/ca, δ18O and δ13C from foraminiferal tests. *Palaeogeogr. Palaeoclimatol. Palaeoecol.* 495, 60–71. doi: 10.1016/j.palaeo.2017.12.027

Schmiedl, G., and Mackensen, A. (2006). Multispecies stable isotopes of benthic foraminifers reveal past changes of organic matter decomposition and deepwater

oxygenation in the arabian sea. *Paleoceanography* 21, PA4213. doi: 10.1029/2006PA001284

Schulz, K. G., Riebesell, U., Rost, B., Thoms, S., and Zeebe, R. E. (2006). Determination of the rate constants for the carbon dioxide to bicarbonate inter-conversion in pH-buffered seawater systems. *Mar. Chem.* 100, 53–65. doi: 10.1016/j.marchem.2005.11.001

Shi, W., Xie, Y., Wang, Z., Li, X., and Tong, C. (2013). Characteristics of overpressure distribution and its implication for hydrocarbon exploration in the qiongdongnan basin. *J. Asian Earth Sci.* 66, 150–165. doi: 10.1016/j.jseaes.2012.12.037

Snyder, G. T., Sano, Y., Takahata, N., Matsumoto, R., Kakizaki, Y., and Tomaru, H. (2020). Magmatic fluids play a role in the development of active gas chimneys and massive gas hydrates in the Japan sea. *Chem. Geol.* 535, 119462. doi: 10.1016/j.chemgeo.2020.119462

Staudigel, H., Albarède, F., Blichert-Toft, J., Edmond, J., McDonough, B., Jacobsen, S. B., et al. (1998). Geochemical earth reference model (GERM): Description of the initiative. *Chem. Geol.* 145, 153–159. doi: 10.1016/S0009-2541(97)00141-1

Su, X., Qu, Y., Chen, F., Yang, S., Zhou, Y., Cui, H., et al. (2020). Deep sea benthic foraminifera from the Taixinan Basin and changes of their cold seep microhabitats during the past 50000 years. *Earth Sci. Front.* 27, 255~275. doi: 10.13745/j.esf.sf.2020.6.13

Suess, E. (2014). Marine cold seeps and their manifestations: Geological control, biogeochemical criteria and environmental conditions. *Int. J. Earth Sci.* 103, 1889–1916. doi: 10.1007/s00531-014-1010-0

Sun, T., Wu, D., Yang, F., Liu, L., Chen, X., and Ye, Y. (2019). Sedimentary geochemical proxies for methane seepage at site C14 in the qiongdongnan basin in the northern south China sea. *Acta Oceanol. Sin.* 38, 84–95. doi: 10.1007/s13131-019-1460-6

Teichert, B. M. A., Gussone, N., Eisenhauer, A., and Bohrmann, G. (2005). Clathrites: Archives of near-seafloor pore-fluid evolution (d44/40Ca, d13C, d18O) in gas hydrate environments. *Geology* 33, 213–216. doi: 10.1130/G21317.1

Tetard, M., Beaufort, L., and Licari, L. (2017). A new optical method for automated pore analysis on benthic foraminifera. *Mar. Micropaleontol.* 136, 30–36. doi: 10.1016/j.marmicro.2017.08.005

Them, T. R., Gill, B. C., Caruthers, A. H., Gerhardt, A. M., Gröcke, D. R., Lyons, T. W., et al. (2018). Thallium isotopes reveal protracted anoxia during the toarcian (early jurassic) associated with volcanism, carbon burial, and mass extinction. *Proc. Natl. Acad. Sci.* 115, 6596–6601. doi: 10.1073/pnas.1803478115

Torres, M. E., Wallmann, K., Tréhu, A. M., Bohrmann, G., Borowski, W. S., and Tomaru, H. (2004). Gas hydrate growth, methane transport, and chloride enrichment at the southern summit of hydrate ridge, cascadia margin off oregon. *Earth Planet. Sci. Lett.* 226, 225–241. doi: 10.1016/j.epsl.2004.07.029

Uchida, T., Ebinuma, T., and Narita, H. (2000). Observations of CO2-hydrate decomposition and reformation processes. *J. Cryst. Growth* 217, 189–200. doi: 10.1016/S0022-0248(00)00470-X

Urey, H. C. (1948). Oxygen isotopes in nature and in the laboratory. *Science.* 108, 489–496. doi: 10.1126/science.108.2810.489

Waelbroeck, C., Labeyrie, L., Michel, E., Duplessy, J. C., McManus, J. F., Lambeck, K., et al. (2002). Sea-level and deep water temperature changes derived from benthic foraminifera isotopic records. *Quat. Sci. Rev.* 21, 295–305. doi: 10.1016/S0277-3791(01)00101-9

Wan, Z., Chen, C., Liang, J., Zhang, W., Huang, W., and Su, P. (2020). Hydrochemical characteristics and evolution mode of cold seeps in the qiongdongnan basin, south China sea. *Geofluids* 2020, 1–16. doi: 10.1155/2020/4578967

Wan, S., Feng, D., Chen, F., Zhuang, C., and Chen, D. (2018). Foraminifera from gas hydrate-bearing sediments of the northeastern south China sea: Proxy evaluation and application for methane release activity. *J. Asian Earth Sci.* 168, 125–136. doi: 10.1016/j.jseaes.2018.04.036

Wan, S., and Jian, Z. (2014). Deep water exchanges between the south China sea and the pacific since the last glacial period. *Paleoceanography* 29, 1162–1178. doi: 10.1002/2013PA002578

Wang, B., Lei, H., Huang, F., Kong, Y., Pan, F., Cheng, W., et al. (2020). Effect of sea-level change on deep-sea sedimentary records in the northeastern south China sea over the past 42 kyr. *Geofluids* 2020, 8814545. doi: 10.1155/2020/8814545

Wang, X., Li, N., Feng, D., Hu, Y., Bayon, G., Liang, Q., et al. (2018). Using chemical compositions of sediments to constrain methane seepage dynamics: A case study from haima cold seeps of the south China sea. *J. Asian Earth Sci.* 168, 137–144. doi: 10.1016/j.jseaes.2018.11.011

Wang, Z., Sun, Z., Zhu, J., Guo, M., and Jiang, R. (2015). Natural gas geological characteristics and great discovery of large gas fields in deep-water area of the western south China sea. *Nat. Gas. Ind. B.* 2, 489–498. doi: 10.1016/j.ngib.2016.03.001

Wang, Z., Wu, X., Wang, L., Song, T., and Hu, Q. (2024). Mechanism of methane migration in oceanic hydrate system: Insights from microfluidic investigations. *Mar. Pet. Geol.* 162, 106743. doi: 10.1016/j.marpetgeo.2024.106743

Wang, S., Yan, B., and Yan, W. (2013). Tracing seafloor methane emissions with benthic foraminifera in the baiyun sag of the northern south China sea. *Environ. Earth Sci.* 70, 1143–1150. doi: 10.1007/s12665-012-2201-2

Watanabe, Y., Nakai, S., Hiruta, A., Matsumoto, R., and Yoshida, K. (2008). U–th dating of carbonate nodules from methane seeps off joetsu, eastern margin of Japan sea. *Earth Planet. Sci. Lett.* 272, 89–96. doi: 10.1016/j.epsl.2008.04.012

Wei, G.-J., Huang, C.-Y., Wang, C.-C., Lee, M.-Y., and Wei, K.-Y. (2006). High-resolution benthic foraminifer δ13C records in the south China sea during the last 150 ka. *Mar. Geol.* 232, 227–235. doi: 10.1016/j.margeo.2006.08.005

Wei, D., Jinqiang, L., Wei, Z., Zenggui, K., Tong, Z., and Yulin, H. (2021). Typical characteristics of fracture-filling hydrate-charged reservoirs caused by heterogeneous fluid flow in the Qiongdongnan Basin, northern south China sea. *Mar. Pet. Geol.* 124, 104810. doi: 10.1016/j.marpetgeo.2020.104810

Wei, J., Liang, J., Lu, J., Zhang, W., and He, Y. (2019). Characteristics and dynamics of gas hydrate systems in the northwestern South China Sea - Results of the fifth gas hydrate drilling expedition. *Mar. Pet. Geol.* 110, 287–298. doi: 10.1016/j.marpetgeo.2019.07.028

Wei, J., Wu, T., Miao, X., and Su, P. (2022). Massive natural gas hydrate dissociation during the penultimate deglaciation (~130 ka) in the south China sea. *Front. Mar. Sci.* 9. doi: 10.3389/fmars.2022.875374

Weldeab, S., Schneider, R. R., Yu, J., and Kylander-Clark, A. (2022). Evidence for massive methane hydrate destabilization during the penultimate interglacial warming. *Proc. Natl. Acad. Sci.* 119, e2201871119. doi: 10.1073/pnas.2201871119

Westbrook, G. K., Thatcher, K. E., Rohling, E. J., Piotrowski, A. M., Pälike, H., Osborne, A. H., et al. (2009). Escape of methane gas from the seabed along the west spitsbergen continental margin. *Geophysical Research Letters* 36, L15608. doi: 10.1029/2009GL039191

Wollenburg, J. E., Raitzsch, M., and Tiedemann, R. (2015). Novel high-pressure culture experiments on deep-sea benthic foraminifera — evidence for methane seepage-related δ13C of *cibicides wuellerstorfi*. *Mar. Micropaleontol.* 117, 47–64. doi: 10.1016/j.marmicro.2015.04.003

Xie, Y., Huang, Y., Feng, J., Wu, G., Xu, Z., Zhang, Z., et al. (2024). Experimental and modeling investigations on CH4 hydrate phase equilibria in multi-ion "haima" cold seep environment. *Gas. Sci. Eng.* 128, 205362. doi: 10.1016/j.jgsce.2024.205362

Xu, C., Wu, N., Sun, Z., Zhang, X., Geng, W., Cao, H., et al. (2021). Assessing methane cycling in the seep sediments of the mid-Okinawa Trough: Insights from pore-water geochemistry and numerical modeling. *Ore. Geol. Rev.* 129, 103909. doi: 10.1016/j.oregeorev.2020.103909

Yang, J., Lu, M., Yao, Z., Wang, M., Lu, S., Qi, N., et al. (2021). A geophysical review of the seabed methane seepage features and their relationship with gas hydrate systems. *Geofluids* 2021, 9953026. doi: 10.1155/2021/9953026

Yang, Y., Xiang, R., Zhang, L., Zhong, F., and Zhang, M. (2020). Is the upward release of intermediate ocean heat content a possible engine for low-latitude processes? *Geology* 48, 579–583. doi: 10.1130/G47271.1

Ye, J., Wei, J., Liang, J., Lu, J., Lu, H., and Zhang, W. (2019). Complex gas hydrate system in a gas chimney, South China Sea. *Mar. Pet. Geol.* 104, 29–39. doi: 10.1016/j.marpetgeo.2019.03.023

Ye, H., Yang, T., Zhu, G., Jiang, S., and Wu, L. (2016). Pore water geochemistry in shallow sediments from the northeastern continental slope of the South China sea. *Mar. Pet. Geol.* 75, 68–82. doi: 10.1016/j.marpetgeo.2016.03.010

Yoo, D. G., Kang, N. K., Yi, B. Y., Kim, G. Y., Ryu, B. J., Lee, K., et al. (2013). Occurrence and seismic characteristics of gas hydrate in the ulleung basin, east sea. *Mar. Pet. Geol.* 47, 236–247. doi: 10.1016/j.marpetgeo.2013.07.001

You, C.-F., Gieskes, J. M., Lee, T., Yui, T.-F., and Chen, H.-W. (2004). Geochemistry of mud volcano fluids in the Taiwan accretionary prism. *Appl. Geochem.* 19, 695–707. doi: 10.1016/j.apgeochem.2003.10.004

Zhang, G., Cao, J., Deng, Y., Lai, H., Jiang, X., Fang, Y., et al. (2023a). A 209,000-year-old history of methane seepage activity controlled by multiple factors in the south China sea. *Mar. Pet. Geol.* 151, 106200. doi: 10.1016/j.marpetgeo.2023.106200

Zhang, Y., Du, Z., Xi, S., Ma, L., Luan, Z., and Zhang, X. (2024). Experimental study on the cold-seep methane hydrate formation kinetics. *Chem. Eng. Sci.* 295, 120144. doi: 10.1016/j.ces.2024.120144

Zhang, J., Lei, H., Chen, Y., Kong, Y., Kandasamy, S., Ou, W., et al. (2018). Carbon and oxygen isotope composition of carbonate in bulk sediment in the southwest Taiwan basin, south China sea: Methane hydrate decomposition history and its link to mud volcano eruption. *Mar. Pet. Geol.* 98, 687–696. doi: 10.1016/j.marpetgeo.2018.08.031

Zhang, W., Liang, J., Lu, J., Meng, M., He, Y., Deng, W., et al. (2020). Characteristics and controlling mechanism of typical leakage gas hydrate reservoir forming system in the Qiongdongnan Basin, northern South China Sea. *Natural Gas. Industry.* 40, 90–99. doi: 10.3787/j.issn.1000-0976.2020.08.007

Zhang, W., Liang, J., Su, P., Wei, J., Gong, Y., Lin, L., et al. (2019a). Distribution and characteristics of mud diapirs, gas chimneys, and bottom simulating reflectors associated with hydrocarbon migration and gas hydrate accumulation in the qiongdongnan basin, northern slope of the south China sea. *Geol. J.* 54, 3556–3573. doi: 10.1002/gj.3351

Zhang, Y., Luo, M., Hu, Y., Wang, H., and Chen, D. (2019b). An areal assessment of subseafloor carbon cycling in cold seeps and hydrate-bearing areas in the northern south China sea. *Geofluids* 2019, 2573937. doi: 10.1155/2019/2573937

Zhang, Y., Xi, S., Du, Z., Luan, Z., and Zhang, X. (2023b). Influence of cold-seep environments on the kinetics of methane hydrate formation. *Mar. Pet. Geol.* 155, 106401. doi: 10.1016/j.marpetgeo.2023.106401

Zhao, S., Liu, Z., Chen, Q., Wang, X., Shi, J., Jin, H., et al. (2017). Spatiotemporal variations of deep-sea sediment components and their fluxes since the last glaciation in the northern south China sea. *Sci. China Earth Sci.* 60, 1368–1381. doi: 10.1007/s11430-016-9058-6

Zhao, Z., Sun, Z., Wang, Z., Sun, Z., Liu, J., and Zhang, C. (2015). The high resolution sedimentary filling in qiongdongnan basin, northern south China sea. *Mar. Geol.* 361, 11–24. doi: 10.1016/j.margeo.2015.01.002

Zheng, Z., Cao, Y., and Chen, D. (2017). Prediction of the methane supply and formation process of gay hydrate reservoir at ODP1247, Hydrate Ridge. *Chin. J. Geophys.* 60, 3167–3176. doi: 10.6038/cjg20170823